Food and Chemical Toxicology 101 (2017) 15–35

Contents lists available at ScienceDirect

Food and Chemical Toxicology

journal homepage: www.elsevier.com/locate/foodchemtox

Comparative systems toxicology analysis of cigarette smoke and aerosol from a candidate modified risk tobacco product in organotypic human gingival epithelial cultures: A 3-day repeated exposure study

Filippo Zanetti [a, *], Bjoern Titz [a], Alain Sewer [a], Giuseppe Lo Sasso [a], Elena Scotti [a], Walter K. Schlage [b], Carole Mathis [a], Patrice Leroy [a], Shoaib Majeed [a], Laura Ortega Torres [a], Brian R. Keppler [c], Ashraf Elamin [a], Keyur Trivedi [a], Emmanuel Guedj [a], Florian Martin [a], Stefan Frentzel [a], Nikolai V. Ivanov [a], Manuel C. Peitsch [a], Julia Hoeng [a]

[a] PMI R&D, Philip Morris Products S.A., Quai Jeanrenaud 5, CH-2000 Neuchâtel, Switzerland
[b] Biology Consultant, Max-Baermann-Str. 21, 51429 Bergisch Gladbach, Germany
[c] Metabolon Inc., 617 Davis Drive, Suite 400, Durham, NC, USA

ARTICLE INFO

Article history:
Received 21 October 2016
Received in revised form
1 December 2016
Accepted 20 December 2016
Available online 23 December 2016

Keywords:
Air–liquid interface aerosol exposure
Metabolomics
3Rs
21st century toxicology
Tobacco heating system 2.2
Gingiva

ABSTRACT

Smoking is one of the major lifestyle-related risk factors for periodontal diseases. Modified risk tobacco products (MRTP) offer a promising alternative in the harm reduction strategy for adult smokers unable to quit. Using a systems toxicology approach, we investigated and compared the exposure effects of a reference cigarette (3R4F) and a heat-not-burn technology-based candidate MRTP, the Tobacco Heating System (THS) 2.2. Human gingival epithelial organotypic cultures were repeatedly exposed (3 days) for 28 min at two matching concentrations of cigarette smoke (CS) or THS2.2 aerosol. Results showed only minor histopathological alterations and minimal cytotoxicity upon THS2.2 aerosol exposure compared to CS (1% for THS2.2 aerosol vs. 30% for CS, at the high concentration). Among the 14 proinflammatory mediators analyzed, only 5 exhibited significant alterations with THS2.2 exposure compared with 11 upon CS exposure. Transcriptomic and metabolomic analysis indicated a general reduction of the impact in THS2.2 aerosol-exposed samples with respect to CS (~79% lower biological impact for the high THS2.2 aerosol concentration compared to CS, and 13 metabolites significantly perturbed for THS2.2 *vs.* 181 for CS). This study indicates that exposure to THS2.2 aerosol had a lower impact on the pathophysiology of human gingival organotypic cultures than CS.

© 2017 The Authors. Published by Elsevier Ltd. This is an open access article under the CC BY license (http://creativecommons.org/licenses/by/4.0/).

1. Introduction

Periodontal diseases are inflammatory disorders that may lead to the destruction of periodontal tissues and eventually tooth loss. One of the major lifestyle-related risk factors for these diseases is smoking (Genco and Borgnakke, 2013). It is reported in several *in vitro* and *in vivo* studies that smoking can induce oxidative stress (D'aiuto et al., 2010, Chapple et al., 2007; Tsai et al., 2005; Carnevali et al., 2003), increase inflammatory responses and reduce the immune response to microorganisms (Genco, 1996; James et al., 1999), and ultimately alter the structure of the mucosal epithelium at the surface of the gingiva (Coppe et al., 2008; Semlali et al., 2011; Villar and de Lima, 2003). The risk for a destructive periodontal disease can be 5- to 20-fold greater for a smoker compared with a person who has never smoked (Bergstrom, 2004).

While stopping smoking would clearly avoid further smoke-related challenge and damage to the gingival epithelium as well as to the respiratory tract and other organ systems such as the blood vessels and the heart, not all adult smokers are able or willing to quit. For these smokers, harm reduction through the development of Modified Risk Tobacco Products (MRTP), such as e-cigarettes and tobacco-heating devices, provides a promising opportunity to deliver nicotine in an aerosol that contains less harmful and potentially harmful constituents (HPHCs) than smoke

* Corresponding author.
E-mail address: filippo.zanetti@pmi.com (F. Zanetti).

http://dx.doi.org/10.1016/j.fct.2016.12.027
0278-6915/© 2017 The Authors. Published by Elsevier Ltd. This is an open access article under the CC BY license (http://creativecommons.org/licenses/by/4.0/).

from a tobacco burning cigarette (Rodu, 2011; Mejia et al., 2010; Sweanor et al., 2007; Zeller et al., 2009; Stratton et al., 2001). Specifically, the U.S. Family Smoking Prevention and Tobacco Control Act defines a Modified Risk Tobacco Product (MRTP) as any tobacco product that is sold or distributed for use to reduce harm or the risk of tobacco related disease associated with commercially marketed tobacco products (Family Smoking Prevention And Tobacco Control ACT, 2009).

The Tobacco Heating System (THS) 2.2[1] is such a candidate Modified Risk Tobacco Product (MRTP), developed by Philip Morris International, which is based on heating, rather than burning, specifically designed tobacco sticks (Smith et al., 2016). Because of the prevention of combustion, the THS2.2 aerosol contains greatly reduced levels of the harmful and potentially harmful constituents found in CS (Phillips et al., 2015; Schaller et al., 2016).

Over the past years, there has been a tremendous effort to substitute animal models with *in vitro* experimental systems, in line with the 3Rs principle (replacement, reduction, and refinement) (Balls, 2010; Flecknell, 2002; Russell et al., 1959). For the *in vitro* study of biological processes in the gingival epithelium, human gingival epithelial organotypic cultures have been developed, in which normal human gingival keratinocytes form a fully differentiated three-dimensional epithelial tissue (EpiGingival™; MatTek, Ashland, MA, USA) (Hai et al., 2006). Several aspects of the *in vivo* situation are recapitulated by these gingival cultures: EpiGingival™ cultures resemble the *in vivo* paradigm under cytomegalovirus infection (Hai et al., 2006), they show good reproducibility of the human situation for carcinogenic studies (Agrawal et al., 2013; Mitchell et al., 2012), and they are suitable for oral care product testing (Yang et al., 2011). In a recent study, we found that gingival cultures also recapitulate several effects of *in vivo* CS exposure, including the release of inflammatory mediators and activation of cell stress networks (Schlage et al., 2014).

In the present study, we compared how THS2.2 aerosol and CS affect the gingival epithelium of the EpiGingival™ system. To better mimic the *in vivo* situation, the gingival cultures were expose to cigarette smoke (CS) or the THS2.2 aerosol at the air-liquid interface using a dedicated aerosol generation and exposure equipment (Vitrocell). We assessed the impact of repeated (3 days) exposure at comparable concentrations of CS and THS2.2 aerosol matched by delivered nicotine dose. The endpoints of our systems toxicology approach included cytotoxicity, histopathology, inflammatory mediators, and molecular investigations using transcriptomics (mRNA and miRNA) and metabolomics – complemented by computational network biology analyses.

Overall, our findings elucidated the complex biological responses of gingival cultures to CS exposure in the EpiGingival™ model, providing evidence that the THS2.2 aerosol has lower biological effects than 3R4F CS on histopathology, gene expression, inflammatory mediator secretion, and oxidative-stress related metabolism.

2. Materials and methods

2.1. Vitrocell® 3R4F smoke and THS2.2 aerosol exposure

Two items were used for the exposures administered in this study: 3R4F cigarettes (reference item) (University of Kentucky, Kentucky Tobacco Research and Development Center, www.ca.uky.edu/refcig) and THS2.2 sticks (test item) (PMI R&D, Neuchâtel, Switzerland). 3R4F cigarettes and THS2.2 sticks were conditioned for at least 48 h and up to 21 days at 22 ± 1 °C with a relative humidity of 60± 3%, according to ISO standard 3402 (International Organization for Standardization, 1999).

CS was generated from 3R4F reference cigarettes and the test aerosol was generated from THS2.2, each inserted into a dedicated 30-port carousel smoking machine SM 2000 (PMI R&D, Neuchâtel, Switzerland). For each exposure run, 10 3R4F cigarettes were smoked for 10–11 puffs each to a standard butt length (approximately 35 mm) and 10 THS2.2 sticks were aerosolized up to 12 puffs each. These conditions were in accordance with the Health Canada smoking regimen, with a 55 mL puff over 2 s, twice per min, with an 8 s pump exhaust time (Health Canada, 1999).

3R4F CS or THS2.2 aerosol exposures were conducted via two separate Vitrocell® 24/48 dilution and exposure systems (Vitrocell 24/48 for 24 well sized inserts; Vitrocell Systems GmbH, Waldkirch, Germany). Inserts were placed in the climatic chamber of the Vitrocell® exposure system and directly exposed to diluted 3R4F CS or THS2.2 aerosol. Dilution was achieved with filtered air conditioned to 60% relative humidity in the dilution and distribution systems, as illustrated in Fig. S1.

A dose range finding (DRF) experiment, metabolomics investigations, and three experimental repetitions were performed over a period of 4 months. For each repetition of the study, three 28-min exposures were performed over 3 days, one per day. For a given exposure run, a paired design was implemented in which the samples were exposed together with their corresponding air controls during each exposure run (Fig. S1). Various endpoints were measured for each group at different time points (Fig. 1).

2.2. Organotypic culture model

The human gingival epithelial organotypic culture model EpiGingival™ (Gin-100) was purchased from MatTek (Ashland, MA, USA). Undifferentiated epithelial cells were used to construct the EpiGingival™ models. The gingival epithelial cells used throughout the study were isolated from the same donor, a healthy non-smoking male, age 46 years.

Upon delivery, gingival cultures had been grown for 14 days after seeding. In order to complete the differentiation at the air–liquid interface according to the supplier's instructions, the organotypic cultures were maintained in-house in fresh medium (GIN-100-DM4a; MatTek) at 37 °C for 3 days before the exposure experiments. After differentiation, organotypic cultures were incubated in maintenance medium (GIN-100-MM; MatTek). Cells were submersed in 100 μL phosphate buffered saline (PBS) on the apical side, to mimic the moistening of saliva *in vivo* (Moharamzadeh et al., 2009), and cultured with 0.7 mL medium in 24-well plates with Transwell® inserts (6.5 mm diameter, 0.4 μm pore size; Greiner Bio-One, Monroe, NC, USA). Both media used in the study (differentiation and maintenance) were produced by MatTek and their composition has not been disclosed. 3 days after arrival, organotypic cultures were exposed to 3R4F CS or THS2.2 aerosol according to the experimental design (Fig. 1).

Cultures were maintained until the following exposure (24 h) or the final collection (4 h or 24 h post exposure) without changing the medium and PBS; for the adenylate kinase (AK) assay and collection of proinflammatory markers, medium was collected and frozen before the second and third exposure and at the final collection time point. The integrity of cultures was assessed microscopically throughout the study by assessing hematoxylin/eosin stained incubator controls at different days during the week of experiment.

[1] THS is a patented novel tobacco product with the commercial name of iQOS™.

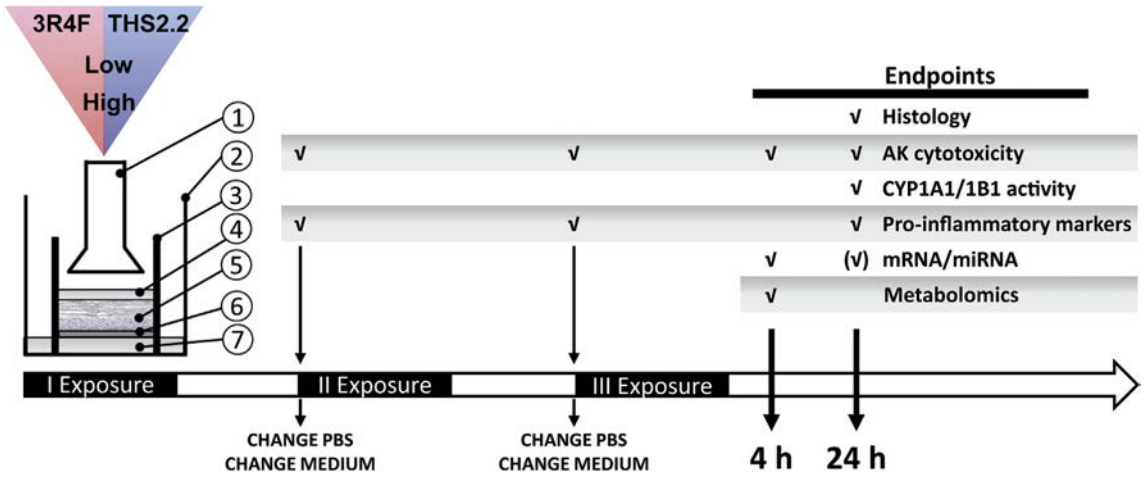

Fig. 1. Study design. Human gingival epithelial organotypic cultures were exposed for 3 consecutive days to 28 min 3R4F CS or THS2.2 aerosol at two matching concentrations. Before each exposure, basolateral medium was collected for different assays (AK and cytokine assays) and replaced with fresh medium; apical PBS was replaced before each exposure. Different endpoints were analyzed at the indicated time points during three experimental repetitions (with three independent exposure runs each, n = 9 total). (✓) for 24 h mRNA/miRNA endpoint indicates that only one experimental repetition (n = 3) was performed. 1, aerosol inlet; 2, culture well; 3, culture insert; 4, apical PBS; 5, organotypic culture; 6, membrane; 7, medium.

2.3. Matching of 3R4F CS and THS2.2 aerosol concentrations by deposited nicotine amount

We used nicotine as the internal reference compound to compare and normalize the concentrations of THS2.2 aerosol with those of 3R4F CS. Nicotine deposition was measured in CS-/aerosol-exposed PBS samples. Briefly, 100 μL PBS was placed into steel inserts and exposed for 28 min to 3R4F CS or THS2.2 aerosol using the Vitrocell® system. Nicotine concentrations were measured using liquid chromatography (LC)–high-resolution accurate-mass–mass spectrometry (MS) (Q Exactive™; Thermo Fisher Scientific, Waltham, MA, USA). Nicotine quantitation was performed using isotopic dilution technique with nicotine-(methyl-d3) as internal standard.

To derive nicotine-matched concentrations of 3R4F CS and THS2.2 aerosol, the amounts of PBS-deposited nicotine were measured in a DRF experiment in which different concentrations/dilutions of 3R4F CS and THS2.2 aerosol were tested. From this, two 3R4F CS and two THS2.2 aerosol concentrations were selected based on histopathological modifications and cytotoxicity, each pair-matched for the delivered nicotine doses. By diluting 3R4F CS with air to 25% we obtained an average concentration of 49.4 mg nicotine/L, corresponding to a delivered dose of 4.94 μg nicotine/100 μL PBS (or μg/insert, being the insert covered by 100 μL PBS). This concentration, indicated in the text as 3R4F (Low) was selected to induce limited cell damage and to support a more detailed investigation of toxicity-related mechanisms associated with exposure (Davis et al., 2013); THS2.2 aerosol was diluted with air to 75%, resulting in a delivered dose of 5.46 μg nicotine/insert (THS2.2 (Low)). For the high matching concentrations, 3R4F CS was diluted to 35% yielding a deposited dose of 8.46 μg nicotine/insert (3R4F (High)). This concentration was selected to cause marked histological alterations and to allow for investigations of what is observed at the earlier 4 h time point at the gene transcription level. THS2.2 aerosol was applied undiluted (100%) corresponding to 10.04 μg nicotine/insert (THS2.2 (High)). The respective sham groups for 3R4F and THS2.2 are defined as 3R4F (Air) or THS2.2 (Air) (Table 1).

2.4. Deposited carbonyls in the Vitrocell® base module following 3R4F CS and THS2.2 aerosol exposures

Carbonyls were measured in PBS following a 28-min exposure to smoke or aerosol, 10 sticks per item, according to the Health Canada smoking regimen described above. Briefly, before exposure, each row in the cultivation base module of the Vitrocell® 24/48 was filled with 18.5 mL PBS. Following exposure to a range of 3R4F CS and THS2.2 aerosol concentrations, acetaldehyde, acetone, acrolein, methyl ethyl ketone, crotonaldehyde, and propionaldehyde were measured in a 1.2 mL aliquot collected from each PBS-exposed sample (per row) and analyzed by high-performance LC coupled with tandem MS, as previously reported (Majeed et al., 2014) (Fig. S2).

2.5. AK-based cytotoxicity assay

AK release was used as a marker of cytotoxicity. AK was sampled in a set of inserts 24 h after the first and second exposure sessions and 4 h after the third or, in another set of inserts, 24 h after the first, second and third exposure, according to the study design (Fig. 1). Cell viability was assessed in basolateral medium of 3R4F CS-exposed and THS2.2 aerosol-exposed organotypic cultures using an AK assay kit (ToxiLight™ bioassay kit; Lonza, Rockland, MA, USA) according to the manufacturer's instructions. Luminescence signals were measured with a FluoStar Omega reader (BMG Labtech GmbH, Ortenberg, Germany). The three aliquots collected at different time points were measured independently and then the values of AK summed to indicate cumulative cytotoxicity through the whole experimental session. AK values were calculated by normalizing the average of the positive control (cultures treated with 1% Triton X-100 for 24 h at the basolateral side) and the negative control (untreated cultures). AK values from samples treated with 1% Triton X-100 were considered as 100% cytotoxicity (complete lysis of cells).

2.6. Histological analysis

Histological assessment was performed 24 h after the last exposure to 3R4F CS or THS2.2 aerosol. Organotypic cultures were

Table 1
Selected CS/aerosol concentrations and matching to delivered nicotine doses.

Group	Name reported	Smoke/aerosol concentration (%)	Nicotine concentration measured in PBS (mg/L; average ± SEM)	Nicotine dose deposited in 100 μL PBS (μg/insert/28 min; average ± SEM)
3R4F low concentration	3R4F (Low)	25	49.4 ± 1.89	4.94 ± 0.189
3R4F high concentration	3R4F (High)	35	84.6 ± 1.43	8.46 ± 0.143
THS2.2 low concentration	THS2.2 (Low)	75	54.6 ± 2.60	5.46 ± 0.260
THS2.2 high concentration	THS2.2 (High)	100	100.4 ± 4.83	10.04 ± 0.483

washed three times with PBS and fixed for 2 h in freshly prepared 4% (w/v) paraformaldehyde. They were washed again at room temperature, both apically and basally, three times with PBS once fixation was completed. After this process, fixed cultures were separated from the inserts by detaching the membrane from the plastic with forceps and were bisected through the middle. Sections were then processed with a Leica ASP300S tissue processor (Leica Biosystem Nussloch GmbH, Nussloch, Germany). The two bisected pieces/sample were embedded into one paraffin block. Five μm-thick sections were obtained using a microtome and mounted on glass slides. Slides were then transferred to an automated slide stainer (Leica ST5020; (Leica Biosystem Nussloch GmbH)). Sections were stained with a standard hematoxylin (Merck Millipore, Schaffhausen, Switzerland) and eosin (Sigma-Aldrich, St. Louis, MO, USA) (H&E) procedure. The stained slides were covered with a glass coverslip using a Leica CV5030 fully automated coverslipper (Leica Biosystem Nussloch GmbH).

For immunohistochemical staining, slides were incubated at 60 °C for a minimum of 30 min. They were then transferred to a Leica Bond-Max autostainer for immunohistochemistry using a Leica Bond™ polymer refine detection kit (#DS9800; Leica Biosystem Nussloch GmbH). Slides were treated with ethylenediaminetetraacetic acid, incubated with an E-cadherin antibody (undiluted PA0387; Leica Biosystem Nussloch GmbH) and counterstained with hematoxylin.

Three slides per condition/experimental replicate were stained. A Hamamatsu NanoZoomer slide scanner (Hamamatsu Photonics, K.K., Japan) was used to generate digital images of each slide. Images were acquired at 10 ×, 63 × and 100 × magnification. The digital images of the hematoxylin and eosin-stained sections were independently assessed in a blinded manner by a certified pathology. The findings were reported in a descriptive manner.

2.7. Cytochrome P450 (CYP) activity

The activity (combined) of cytochrome P450 (CYP) 1A1/1B1 was measured 24 h after the last exposure in basolateral medium of gingival cultures using the P450-Glo™ assay (Promega, Madison, WI, USA), according to the manufacturer's instructions. Briefly, organotypic cultures were incubated for 24 h prior to sample collection in medium with luminogenic luciferin-CEE, a substrate for both CYP1A1 and CYP1B1. For this reason, it was not possible to measure CYP1A1/1B1 activity at the 4 h post exposure time point. Light was emitted upon addition of the luciferin detection reagent and quantified after a 20-min incubation at room temperature in a FluoStar Omega reader (BMG Labtech GmbH). For each of the three experimental repetitions, three organotypic culture inserts were treated with 30 nM 2,3,7,8-tetrachlorodibenzo-p-dioxin (TCDD) as a positive control, added to the basolateral medium 48 h before sample collection and replenished after 24 h. Three other inserts per experimental repetition were treated with PBS in basolateral medium for use as a negative control (0% activity).

2.8. Metabolomics data generation and analysis

Metabolomics was performed in collaboration with Metabolon (Durham, NC, USA). Briefly, organotypic cultures were exposed to fresh air, 3R4F CS (High), and THS2.2 aerosol (High). For each sample, five organotypic cultures were pooled to obtain sufficient cellular material for the assay (approximately 25 mg). The assay was performed in five replicates (i.e. five separate exposure repetitions for each sample type) and metabolic alterations were measured 4 h after the last exposure using Metabolon's global untargeted biochemical profiling platform. More details are given in the Supplementary Materials and Methods; an earlier version of the profiling platform was described by Evans et al. (2009). Briefly, metabolites were extracted from each sample (normalized by tissue weight) with methanol and analyzed with four different MS-based methods: two separate reverse phase (RP)/ultra performance (UP)LC–MS/MS methods with positive ion mode electrospray ionization (ESI), one for analysis by RP/UPLC–MS/MS with negative ion mode ESI, and one for analysis by hydrophilic interaction liquid chromatography/UPLC–MS/MS with negative ion mode ESI. Raw data was extracted, peak-identified, and quality control (QC) processed using Metabolon's software. Peaks were quantified using the area-under-the-curve. A global variance stabilizing normalization of the raw abundance data was performed with the corresponding Bioconductor package in R (Huber et al., 2002; Hultin-rosenberg et al., 2013). Following the common approach taken by Metabolon (Fok et al., 2014; Saito et al., 2016), missing values were assumed to be missing due to low abundance and were imputed as the minimum value separately for each metabolite (Fig. S7A shows the percent imputed values per metabolite). A linear model was fitted for each exposure condition and the corresponding air-exposed group, and p-values from a moderated *t*-statistic were calculated using the empirical Bayes approach (Gentleman et al., 2004). The Benjamini–Hochberg false discovery rate (FDR) method was used to correct for multiple testing effects. Metabolites with an adjusted p-value <0.05 were considered differentially abundant. For comparison, the differential abundance results without imputation are also shown in Fig. S7B. The data is available as Table S4.

2.9. Transcriptomics data generation and analysis

Total RNA from 72 samples was isolated and purified (9 biological replicates for 4 h and 3 biological replicates for 24 h; for six sample groups including paired controls: THS2.2 (Low, High, sham control), 3R4F (Low, High, sham control) (*Supplementary Materials and Methods: RNA and miRNA purification*). The resulting cocktail was successfully hybridized into Affymetrix GeneChip® HG U133 Plus 2.0 arrays for 69 samples to generate CEL files containing the

probe set intensity values (three 3R4F (High) 24 h samples had to be discarded due to too low RNA concentration) (*Supplementary Materials and Methods: mRNA microarrays*). The raw data contained in the CEL files underwent quality controls, discarding three additional CEL files (three 3R4F (High), 4 h samples), before being transformed into the normalized expression matrix used to calculate the gene differential expressions (*Supplementary Materials and Methods: mRNA differential expression calculation*). To perform a comparative systems toxicology assessment of exposures to 3R4F CS and THS2.2 aerosol, a collection of 28 causal biological networks covering the main biological processes in the pulmonary system (Boue et al., 2015) was used, which were *a priori* considered as relevant to capture the response of exposed gingival cultures. Gene differential expression values were computed using the 28 network models to derive the network perturbation amplitude (NPA) and biological impact factor (BIF), which quantify the systems response in terms of network perturbations (Martin et al., 2014) (*Supplementary Materials and Methods: Network-based systems toxicology assessment*). Gene set analysis (GSA) was included as a widely used approach for interpreting gene differential expressions and aimed at confirming and possibly complementing NPA results (*Supplementary Materials and Methods: Gene-set analysis*).

2.10. miRNomics data generation and analysis

Mature microRNAs (miRNAs) from the same 72 samples as for transcriptomics were isolated and purified (*Supplementary Materials and Methods: miRNA purification*). The resulting cocktail was successfully hybridized into Affymetrix GeneChip® miRNA 4.0 arrays for 69 samples to generate the CEL files containing probe set intensity values (three 3R4F (High) 24 h samples had to be discarded due to too low RNA concentration) (*Supplementary Materials and Methods: miRNA microarrays*). The raw data contained in the CEL files underwent quality controls, discarding four additional CEL files (three sham and one 3R4F (Low) 24 h sample), and several detection call-based filtering steps before being transformed into the final normalized expression matrix used to calculate miRNA differential expressions (*Supplementary Materials and Methods: miRNA differential expression calculation*). Three candidate integrated miRNA-mRNA networks for relevant biological processes (oxidative stress, xenobiotic metabolism, and inflammation) were generated through the use of QIAGEN's Ingenuity® Pathway Analysis (IPA®; QIAGEN Redwood City, www.qiagen.com/ingenuity) using the differential expression data (*Materials and Methods: Integrated analysis of miRNA and mRNA expression profiles*). The NPA formula $(1/N_{edges}) \cdot \sum_{miRNA\text{-}mRNA\ edges} (\beta_{miRNA} - \beta_{mRNA})^2$ was evaluated using miRNA and mRNA differential expressions (β_{miRNA} and β_{mRNA}) and the three candidate integrated miRNA-mRNA networks assembled previously. Similarly to the comparative network-based systems toxicology assessment described above, the miRNPA values quantify network-level activity changes between exposed and control sample groups (*Supplementary Materials and Methods: Network-based integrated miRNA-mRNA assessment*).

2.11. Integrated analysis of miRNA and mRNA expression profiles

To determine mRNA-miRNA interactions, we analyzed the target genes of differentially expressed miRNA using QIAGEN's IPA® (QIAGEN Redwood City) tools (version March 2016). We set the cut-off for up-regulated miRNAs at $\geq$1.2-fold change and $\leq$0.83 for down-regulated miRNAs. No significant number of differentially expressed miRNA was found for the low 3R4F CS and THS2.2 aerosol concentrations. Therefore, we decided to use only the high doses of nicotine in 3R4F CS and THS2.2 aerosol, 4 h post exposure. We generated high confidence miRNA target predictions as well as experimentally observed miRNA-mRNA interactions using the IPA® tool called "MicroRNA Target Filter", which integrates multiple target prediction algorithms such as TargetScan, TarBase, miRecords, and the Ingenuity Knowledge Base. Opposite expression pairing between miRNA and mRNA levels was implemented to further refine the analysis. Further filtering options, such as specific tissues/cell lines related to the epidermis, were applied as confidence parameters. The resulting miRNA-mRNA interaction pairs were mapped with the previously identified differentially expressed mRNAs, for which a FDR threshold was set at 0.05. The resulting interaction networks of differentially expressed miRNAs and mRNAs were visualized by IPA®.

To identify the most relevant canonical pathways affected in our biological system, we excluded some pathways not related to gingival biology, these being cancer, cardiovascular signaling, pathogen-influenced signaling, and neurotransmitters and other nervous system signaling. Using the "Build-Path Explorer" option in IPA®, we identified all the relationships among genes and miRNAs in the cluster. The following option was selected: Interactions = Only "direct", and all other options were left as default. Subsequently, using the "Path Designer" tool in IPA® and using the "Overlay-Canonical Pathways" option, we added all the canonical pathways involved in oxidative, xenobiotic, and inflammation stress.

2.12. Luminex-based measurement of secreted analytes

Measurement of secreted proinflammatory mediators was performed 24 h after each exposure session (Fig. 1) by collecting 200-μL aliquots of basolateral medium from organotypic culture inserts. Profiling was done using Luminex® xMAP® technology (Luminex, Austin, TX, USA) with commercially available assay panels (EMD Millipore Corp., Schwalbach, Germany) to detect the following mediators: TNFα, chemokine (C-C motif) ligand (CCL)2, CCL5, colony-stimulating factor (CSF)2, CSF3, IL-6, IL-8, IL-1A, IL-1B, chemokine (C-X-C motif) ligand (CXCL)1, CXCL10 (named also Interferon gamma-induced protein 10 (IP-10)), MMP-1, MMP-9, and vascular endothelial growth factor alpha (VEGFA). The assay was performed according to the manufacturer's instructions. Briefly, 25 μL diluted or undiluted sample was used for each detection and analysis was conducted on a Luminex®, 200™, or FLEXMAP 3D® reader, equipped with xPONENT software (Luminex). Three samples were treated for 24 h with TNFA and IL-1B (each at a 10 ng/mL final concentration) in basolateral medium as a positive control. As a negative control, a second set of triplicate samples was treated for 24 h with PBS in basolateral medium. Positive and negative controls were used fresh for each experimental repetition. Whenever measured concentrations fell below the limit of quantitation, a constant value was used (i.e. half of the lower limit of detection).

2.13. Statistical and reproducibility analysis

Statistical analysis was performed using SAS software version 9.2 (SAS, Wallisellen, Switzerland) on data from AK assays, CYP activities, and Luminex-based measurements of secreted mediators. Mean and standard error of the mean (SEM) values are reported unless otherwise specified. Comparisons of data from an exposed sample *vs.* its air control (i.e. the paired-sample from the same exposure run) were performed using a paired *t*-test. Comparison of data from a tissue exposed to 3R4F CS *vs.* THS2.2 aerosol was performed after appropriate air controls (i.e. using paired samples) had been subtracted, using a *t*-test corrected for non-equal variance (Satterthwaite correction). The raw p-values obtained are reported. Before applying the paired *t*-test to data from

secreted mediator analyses (Luminex assay), values were transformed using natural log transformation.

3. Results

3.1. Effects of 3R4F CS and THS2.2 aerosol on culture viability and morphology

Using a 3-day repeated exposure regime, the effects of 3R4F CS and THS2.2 aerosol on human gingival epithelial organotypic cultures were tested at two pair-matched concentrations by delivered nicotine dose: 4.94 and 8.46 μg nicotine/insert for 3R4F (Low) and 3R4F (High) and 5.46 and 10.04 μg nicotine/insert for THS2.2 (Low) and THS2.2 (High), respectively (Table 1). To mimic the moistening of gingival mucosa in the oral cavity, we wetted the gingival cultures with PBS on the apical side during the experiments (see methods for details).

To assess the effects on cell viability, we measured AK (adenylate kinase) release into basolateral media over the whole period of exposure and 4 and 24 h after the last exposure. The results in Fig. 2A report the cumulative AK release and indicate that gingival cultures were not damaged by either 3R4F CS or THS2.2 aerosol up to 4 h after the last exposure (see also Fig. S3 for AK release results after each exposure). In contrast, cytotoxicity was detected 24 h after the last exposure (Fig. 2B), proportionally to the 3R4F CS concentration applied (nearly 9% for 3R4F (Low) and around 30% for 3R4F (High)); no major cytotoxicity was observed for THS2.2 aerosol-exposed cultures at both concentrations tested.

Epithelia commonly respond to topical irritation challenges through morphological adaptations (e.g., keratinization, metaplasia), while strong irritation and toxicological challenges result in morphologically visible tissue damage. To detect irritation-related morphological alterations due to CS or THS2.2 aerosol exposure, we performed histopathological analysis of the gingival cultures (Fig. 2C). Gingival cultures exposed to air (sham) for both 3R4F and THS2.2 groups maintained the physiological structure of the cornified, stratified squamous epithelium, where distinct cell layers were observable, these being stratum basale, stratum spinosum,

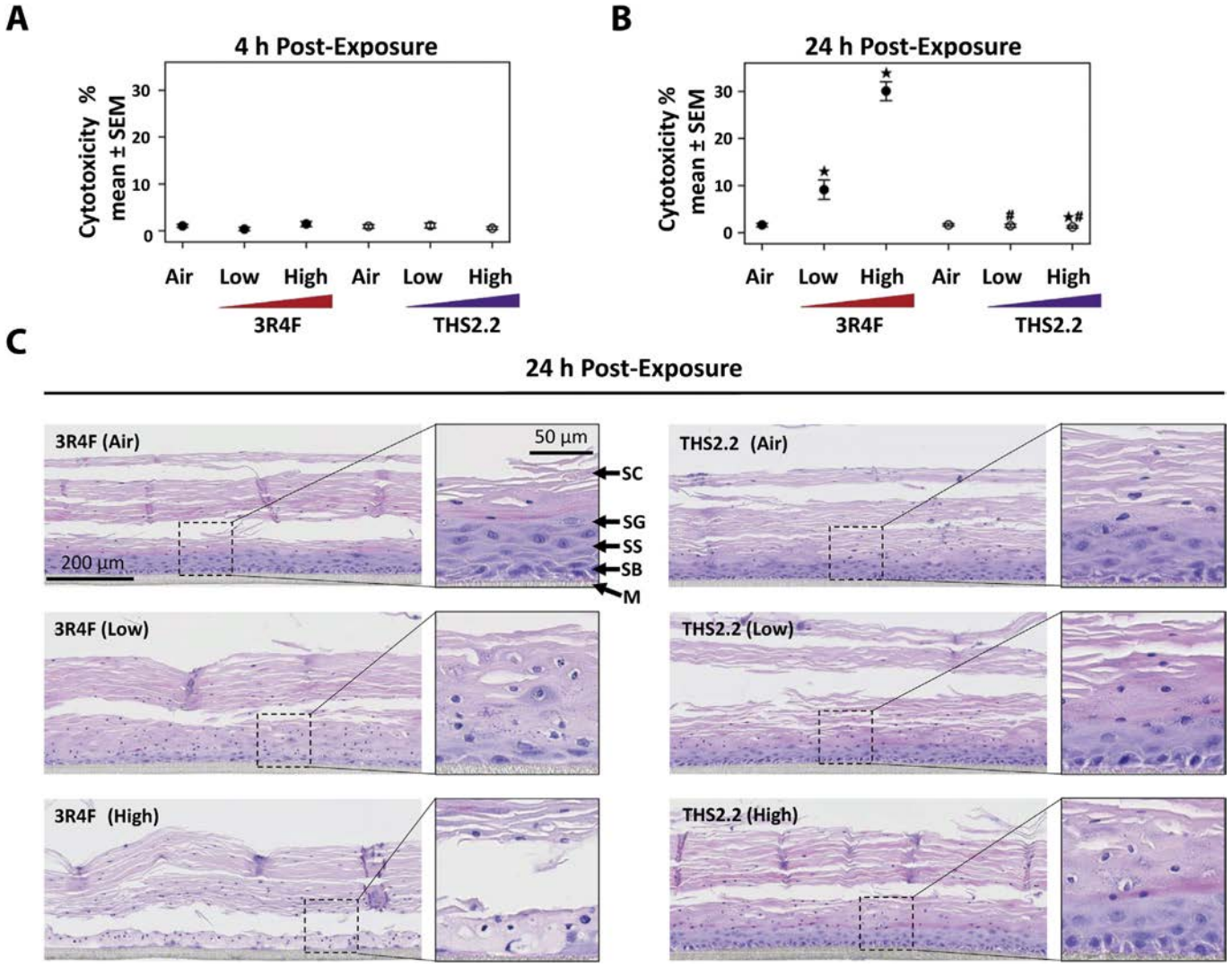

Fig. 2. Cytotoxicity and tissue morphology of organotypic gingival cultures exposed to 3R4F CS and THS2.2 aerosol. Mean cumulative cytotoxicity levels were assessed using the AK assay at 4 h (**A**) and 24 h (**B**) post exposure time points. AK levels were normalized to values of the positive control (Triton-X-treated cultures, considered 100% cytotoxicity). Error bars indicate SEM (n = 9). *p < 0.05, compared with the corresponding air control; #p < 0.05, compared with matching concentrations of 3R4F CS. (**C**) Representative images of H&E-stained gingival cultures after 24 h from the last exposure to 3R4F CS (left) or THS2.2 aerosol (right). Abbreviations indicate different layers of gingival cultures: M, membrane; SB, stratum basale, SS, stratum spinosum; SG, stratum granulosum; SC, stratum corneum. H&E images show 20 × magnification, and 63 × magnification for image insets. n = 9.

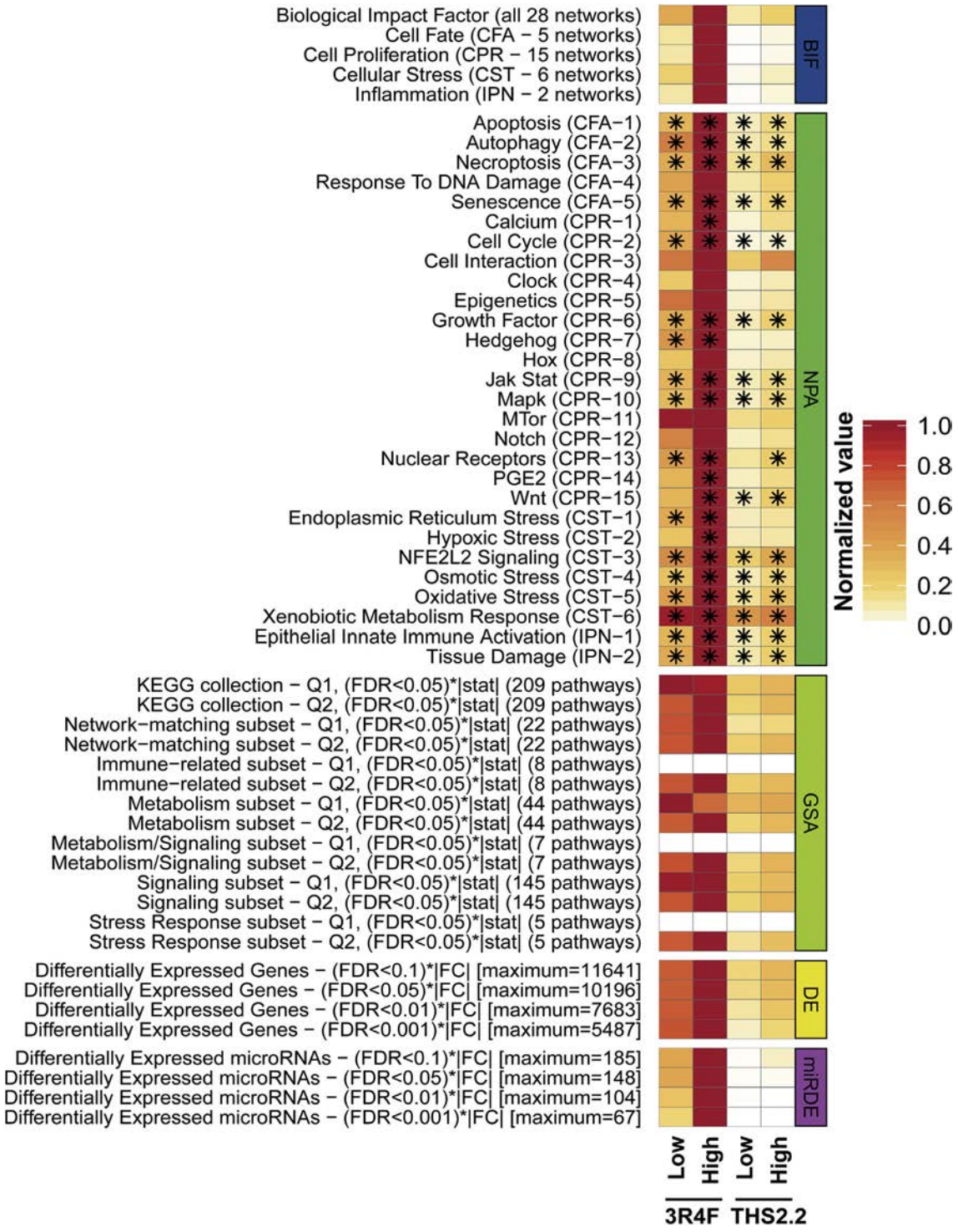

Fig. 3. Overview of the impact of 3R4F CS or THS2.2 aerosol exposures on differential expression of genes. Values are normalized to the interval [0, 1] in a row-wise manner. Details of their calculations and meanings are given in the Materials and Methods section. The uppermost panel displays the biological impact factor (BIF), which quantifies the overall impact of the exposures using the full suite of networks. It also includes the contribution of the four network families to the overall BIF (cell fate and angiogenesis (CFA), cell proliferation (CPR), cellular stress (CST), and pulmonary inflammation (IPN)). The contributions of network families result from aggregation of network perturbation amplitudes (NPA) for each single network; these are shown for each relevant network in the middle panel. The "*" indicates statistically significant network perturbations, as explained in the Materials and Methods section. Overall results of gene set analyses (GSA) are displayed in the next panel for KEGG collection and the two standard statistical tests (Q1 and Q2). Also shown are specific subsets of KEGG collection: first, the 22 pathways matching the mechanistic networks, and second, the five broad categories of the 228 pathways contained in the KEGG collection. To enhance the differences between the columns, displayed values were defined as sums of absolute values of gene set-level statistics (i.e. fold-change mean) for the statistically significant gene sets in each category. The two lower panels show the number of differentially expressed genes (DE) and miRNAs (miRDE) for four distinct statistical significance thresholds, to identify possible threshold effects. Again, sums of absolute values of fold-changes of statistically significant genes or miRNAs are displayed to enhance differences between columns. n = 6–9.

Table 2
List of miRNAs affected by 3R4F CS and THS2.2 aerosol exposure.

3R4F		Symbol	Log2 Ratio 3R4F (High)	
	miRNA up-regulated	miR-149-3p (and other miRNAs w/seed GGGAGGG)	1.069	
		miR-4454 (miRNAs w/seed GAUCCGA)	0.971	
		miR-762 (and other miRNAs w/seed GGGCUGG)	0.776	
		miR-1343-5p (and other miRNAs w/seed GGGGAGC)	0.741	
		miR-150-3p (miRNAs w/seed UGGUACA)	0.740	
		miR-92b-5p (miRNAs w/seed GGGACGG)	0.721	
		miR-572 (miRNAs w/seed UCCGCUC)	0.618	
		miR-292b-5p (and other miRNAs w/seed CUCAAAA)	0.600	
		miR-4734 (miRNAs w/seed CUGCGGG)	0.591	
		miR-4707-5p (miRNAs w/seed CCCCGGC)	0.574	
		miR-4467 (miRNAs w/seed GGCGGCG)	0.568	
		miR-1908-5p (and other miRNAs w/seed GGCGGGG)	0.552	
		miR-1275 (and other miRNAs w/seed UGGGGGA)	0.544	
		miR-4634 (miRNAs w/seed GGCGCGA)	0.491	
		miR-4651 (and other miRNAs w/seed GGGGUGG)	0.485	
		miR-1207-5p (and other miRNAs w/seed GGCAGGG)	0.473	
		miR-3473b (and other miRNAs w/seed GGCUGGA)	0.448	
		miR-3937 (miRNAs w/seed CAGGCGG)	0.448	
		miR-29b-1-5p (miRNAs w/seed CUGGUUU)	0.423	
		miR-4676-5p (and other miRNAs w/seed AGCCAGU)	0.410	
		miR-3648 (miRNAs w/seed GCCGCGG)	0.385	
		miR-320b (and other miRNAs w/seed AAAGCUG)	0.384	
		miR-4690-5p (miRNAs w/seed AGCAGGC)	0.381	
		miR-665 (and other miRNAs w/seed CCAGGAG)	0.357	
		miR-2861 (and other miRNAs w/seed GGGCCUG)	0.323	
		miR-375-3p (and other miRNAs w/seed UUGUUCG)	0.309	
		miR-3187-3p (miRNAs w/seed UGGCCAU)	0.308	
		miR-194-5p (miRNAs w/seed GUAACAG)	0.307	
		miR-4508 (and other miRNAs w/seed CGGGGCU)	0.305	
		miR-3621 (miRNAs w/seed GCGGGUC)	0.296	
		miR-675-5p (and other miRNAs w/seed GGUGCGG)	0.286	
		miR-658 (miRNAs w/seed GCGGAGG)	0.278	
		miR-224-5p (miRNAs w/seed AAGUCAC)	0.274	
		miR-324-5p (miRNAs w/seed GCAUCCC)	0.269	
		miR-24-1-5p (and other miRNAs w/seed GCCUACU)	0.265	
	miRNA down-regulated	miR-30c-5p (and other miRNAs w/seed GUAAACA)	−0.269	
		miR-342-3p (miRNAs w/seed CUCACAC)	−0.432	
		miR-423-3p (miRNAs w/seed GCUCGGU)	−0.466	
		miR-4710 (miRNAs w/seed GGUGAGG)	−0.471	
		miR-125b-5p (and other miRNAs w/seed CCCUGAG)	−0.497	
		miR-3935 (miRNAs w/seed GUAGAUA)	−0.542	
THS2.2		**Symbol**	**Log2 Ratio THS2.2 (High)**	
	miRNA up-regulated	–	–	
	miRNA down-regulated	miR-23a-5p (and other miRNAs w/seed GGGUUCC)	−0.299	
3R4F + THS2.2		**Symbol**	**Log2 Ratio 3R4F (High)**	**Log2 Ratio THS2.2 (High)**
	miRNA up-regulated	miR-4530 (miRNAs w/seed CCAGCAG)	1.75	0.306
		miR-4443 (miRNAs w/seed UGGAGGC)	1.117	0.466
		miR-494-3p (miRNAs w/seed GAAACAU)	0.564	0.37
		miR-642a-3p (and other miRNAs w/seed GACACAU)	0.461	0.275
	miRNA down-regulated	miR-296-3p (miRNAs w/seed AGGGUUG)	−1.835	−0.696
		miR-4669 (miRNAs w/seed GUGUCCG)	−1.505	−0.625
		miR-3141 (miRNAs w/seed AGGGCGG)	−1.415	−0.602
		miR-188-5p (and other miRNAs w/seed AUCCCUU)	−1.27	−0.551
		miR-3682-3p (miRNAs w/seed GAUGAUA)	−1.242	−0.555
		miR-3911 (and other miRNAs w/seed GUGUGGA)	−1.236	−0.576
		miR-4462 (miRNAs w/seed GACACGG)	−1.113	−0.428
		miR-4459 (miRNAs w/seed CAGGAGG)	−0.994	−0.521
		miR-1268a (and other miRNAs w/seed GGGCGUG)	−0.952	−0.387
		miR-1302 (and other miRNAs w/seed UGGGACA)	−0.888	−0.315
		miR-617 (miRNAs w/seed GACUUCC)	−0.862	−0.277
		miR-1306-3p (miRNAs w/seed CGUUGGC)	−0.824	−0.276
		miR-193a-5p (miRNAs w/seed GGGUCUU)	−0.812	−0.273
		miR-4521 (miRNAs w/seed CUAAGGA)	−0.77	−0.368
		miR-1224-5p (and other miRNAs w/seed UGAGGAC)	−0.728	−0.406
		miR-3613-5p (miRNAs w/seed GUUGUAC)	−0.448	−0.281
		miR-4750-5p (miRNAs w/seed UCGGGCG)	−0.324	−0.263

The upper table describes the miRNA impacted only by 3R4F CS, the middle table indicates the miRNA impacted only by THS2.2 aerosol, while the bottom table (3R4F + THS2.2) indicates miRNA regulated by both 3R4F CS and THS2.2 aerosol. Log2 Ratio indicates the logarithm to base 2 of the fold change difference with the respective air control.

stratum granulosum, and stratum corneum. Twenty-four hours post exposure to 3R4F CS, clear histological modifications were observed: at the low 3R4F CS concentration (middle left panel) the distinction between stratum granulosum and stratum corneum

became blurry or completely lost with the presence of keratohyaline granules in both layers; occasional atrophy of the stratum spinosum was observed. At the high 3R4F CS concentration (lower left panel), the tissue models appeared severely damaged, showing complete loss of the stratum spinosum (atrophy), keratinization extending until the stratum basale or even the membrane; overt apoptosis/karyorrhexis/pyknosis was present.

THS2.2 aerosol-exposed samples (Fig. 2C, right panels) showed minor changes, with only sporadic atrophy observed and loss of clear distinction between stratum granulosum and stratum corneum proportional to the THS2.2 aerosol concentration; the morphological alterations observed were clearly less pronounced with respect to the corresponding 3R4F CS-exposed counterparts.

3.2. Biological impact of 3R4F CS and THS2.2 aerosol based on transcriptional changes

Measurement of cytotoxicity using the AK assay indicated that 4 h after the repeated exposures to 3R4F CS and THS2.2 aerosol cell death was very limited; whereas at 24 h, we observed extensive morphological alteration and cytotoxicity following 3R4F CS exposure, (Fig. 2A and B). The absence of overt cell death allows the investigation of toxicity-specific mechanisms associated with exposure, instead of effects reflecting morphological alterations associated only with severely damaged tissue (Davis et al., 2013). Therefore, we focused on the 4 h post exposure time point to measure transcriptional changes and perform a systems toxicology-based assessment of 3R4F CS and THS2.2 aerosol exposures. We also measured transcriptional changes 24 h after the last exposure in a more exploratory manner, as only three replicates were produced (rather than nine) and no data were available for the more toxic high 3R4F CS concentration.

Our pipeline inputting transcriptomic profiles and yielding network-based systems toxicology assessment is based on standard microarray technologies and operates in an open-source computational environment to quantify the systems response in terms of network perturbations (Martin et al., 2014) represented by the BIF and the NPA scores (see Materials and Methods).

The BIF panel illustrated in Fig. 3 quantifies the overall biological impact of 3R4F CS and THS2.2 aerosol and can be broken down into the contributions of four network families (cell fate and angiogenesis (CFA), cell proliferation (CPR), cell stress (CST), and inflammatory process network (IPN)). The heatmap shows that, at both the overall and network-family levels, the impact of 3R4F CS was higher than THS2.2 aerosol, and increasing with CS concentration.

In the NPA panel (Fig. 3) these quantitative results are broken down into the effects of 3R4F CS and THS2.2 aerosol for all networks of the collection (Table S1). The major changes were induced by 3R4F CS exposure and were impacting almost all networks, with a concentration-dependent effect. The most significant alterations were observed for networks belonging to the CFA-, CST-, and IPN-related families. Differently to the other networks, the "Xenobiotic Metabolism Response" network was equally perturbed by the exposures to 3R4F CS low and high concentrations, while the reduction upon exposures to THS2.2 aerosol was less pronounced than for other networks. Some of the networks were exclusively impacted by 3R4F CS, like "Calcium", "Hedgehog", "PGE2", "Endoplasmic Reticulum Stress", and "Hypoxic Stress". Overall, the response to THS2.2 aerosol was always much lower than to 3R4F CS at comparable concentrations, except for the xenobiotic metabolism network.

We completed our network-based systems toxicology assessment by performing common gene-set analysis GSA to confirm and possibly extend the obtained results (see Materials and Methods). GSA involves gene sets covering biological processes that are not necessarily included in the networks used in NPA/BIF calculations and is therefore also suitable for exploratory investigations. We first extracted 22 "confirmatory" KEGG pathways overlapping with key molecules belonging to our network list. Then five broad pathway categories were defined by grouping the 209 KEGG pathways by gene content and biological processes (Zanetti et al., 2016). Two standard GSA statistical tests were applied: the competitive Q1 (permutation of genes) and the self-contained Q2 (permutation of samples) (Nam and Kim, 2008). The GSA panel (Fig. 3) shows that the Q2 results exhibit the same pattern as the network-based systems toxicology results: strong dose-dependent enrichments for gingival cultures exposed to 3R4F CS, whereas exposure to THS2.2 aerosol did not return comparable values. These results support the suitability of the GSA Q2 test as a confirmatory quantification of the biological impact of exposure. They reflect the fact that Q2 specifically tests the association between one gene set and the treatment effects, whereas Q1 compares one gene set with another. A detailed illustration of the 22 network-matching pathways of the KEGG collection can be found in Fig. S4.

The differentially expressed genes shown in the respective panel (DE) of Fig. 3 indicate that the impact of 3R4F CS on gene expression was higher than THS2.2 aerosol at all the concentrations tested. Moreover, the impact on gene expression was concentration-dependent.

Twenty-four hours after the last exposure, the low concentration of 3R4F CS and both concentrations of THS2.2 aerosol were assessed for a reduced number of replicates using our network-based systems toxicology approach to investigate the tissue recovery phase. However, to make fair comparisons between the three replicates at 24 h and the nine replicates at 4 h post exposure, we split the 4 h samples into three groups of three samples matching the batches of the experiment execution (Fig. S5). For the low 3R4F CS concentration, results showed an increase in values of the BIF, the network-family BIFs, and most of the 28 network NPAs with respect to the 4 h post exposure time point. One notable exception is the "Xenobiotic Metabolism Response" network, where a decrease in NPA was observed. For THS2.2 aerosol-exposed samples, all BIF/NPA values were lower. Globally, the lower impact of exposure to THS2.2 aerosol compared with 3R4F CS was confirmed. Interestingly, the differentially expressed gene panel (Fig. 3 and Fig. S5, DE panel) shows decreased values upon the 4 h-to-24 h recovery period for both 3R4F and THS2.2 treatments. This result demonstrates the power of the multivariate network-based approach, which captures collective effects beyond individual gene measurements provided by transcriptomics data. In summary, including the 24 h data indicated that while the CS-exposed cultures showed an exacerbation of the response at 24 h, those exposed to THS2.2 aerosol resulted in a slightly less impacted BIF panel, indicating a recovery trend over time.

The analysis of miRNAs focused on all the networks and highlighted 66 differentially expressed miRNAs (FDR < 0.05), 41 regulated only by 3R4F CS, one miRNA regulated only by THS2.2 aerosol, and 21 commonly regulated by both treatments (Table 2). The number of significantly regulated miRNAs was higher for 3R4F compared with THS2.2 at 4 h post exposure (Fig. 3, miRDE panel), without any differential expression for the low concentration at 24 h post exposure (Fig. S5).

In the next paragraphs, we focus our analysis on selected networks relevant to smoking- and periodontal disease-induced alterations.

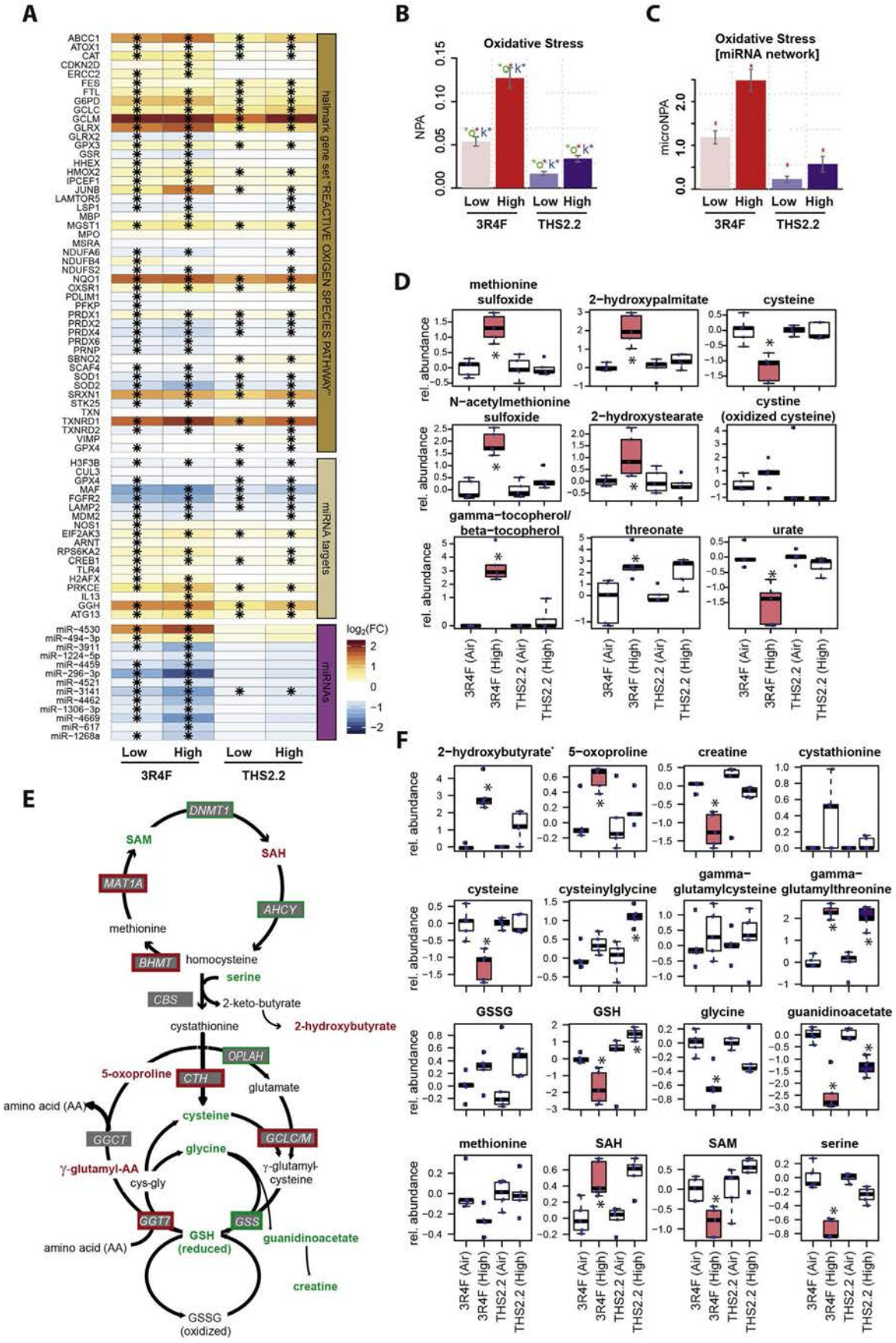
A
ABCC1
ATOX1
CAT
CDKN2D
ERCC2
FES
FTL
G6PD
GCLC
GCLM
GLRX
GLRX2
GPX3
GSR
HHEX
HMOX2
IPCEF1
JUNB
LAMTOR5
LSP1
MBP
MGST1
MPO
MSRA
NDUFA6
NDUFB4
NDUFS2
NQO1
OXSR1
PDLIM1
PFKP
PRDX1
PRDX2
PRDX4
PRDX6
PRNP
SBNO2
SCAF4
SOD1
SOD2
SRXN1
STK25
TXN
TXNRD1
TXNRD2
VIMP
GPX4
hallmark gene set "REACTIVE OXIGEN SPECIES PATHWAY"
H3F3B
CUL3
GPX4
MAF
FGFR2
LAMP2
MDM2
NOS1
EIF2AK3
ARNT
RPS6KA2
CREB1
TLR4
H2AFX
PRKCE
IL13
GGH
ATG13
miRNA targets
miR−4530
miR−494−3p
miR−3911
miR−1224−5p
miR−4459
miR−296−3p
miR−4521
miR−3141
miR−4462
miR−1306−3p
miR−4669
miR−617
miR−1268a
miRNAs
log2(FC)
2
1
0
−1
−2
Low High Low High
3R4F THS2.2
B
Oxidative Stress
NPA
0.00 0.05 0.10 0.15
Low High Low High
3R4F THS2.2
C
Oxidative Stress
[miRNA network]
microNPA
0.0 1.0 2.0
Low High Low High
3R4F THS2.2
D
methionine sulfoxide
2−hydroxypalmitate
cysteine
N−acetylmethionine sulfoxide
2−hydroxystearate
cystine (oxidized cysteine)
gamma−tocopherol/ beta−tocopherol
threonate
urate
rel. abundance
3R4F (Air)
3R4F (High)
THS2.2 (Air)
THS2.2 (High)
E
DNMT1
SAM
SAH
MAT1A
AHCY
methionine
BHMT
homocysteine
serine
CBS
2-keto-butyrate
cystathionine
2-hydroxybutyrate
OPLAH
5-oxoproline
CTH
glutamate
amino acid (AA)
cysteine
GGCT
GCLC/M
glycine
γ-glutamyl-AA
cys-gly
γ-glutamyl-cysteine
GGT7
GSS
GSH (reduced)
guanidinoacetate
amino acid (AA)
creatine
GSSG (oxidized)
F
2−hydroxybutyrate
5−oxoproline
creatine
cystathionine
cysteine
cysteinylglycine
gamma−glutamylcysteine
gamma−glutamylthreonine
GSSG
GSH
glycine
guanidinoacetate
methionine
SAH
SAM
serine
rel. abundance
3R4F (Air)
3R4F (High)
THS2.2 (Air)
THS2.2 (High)

3.3. Oxidative stress response upon 3R4F CS and THS2.2 aerosol exposure

To assess the induction of an acute oxidative stress response, we first evaluated differential gene expression for the reactive oxygen species pathway (Liberzon et al., 2015) 4 h after the third 3R4F CS or THS2.2 aerosol exposure. 3R4F CS broadly affected this pathway, with an especially strong up-regulation of the oxidative stress response genes glutamate-cysteine ligase modifier subunit (*GCLM*), thioredoxin reductase 1 (*TXNRD1*), NAD(P)H quinone dehydrogenase 1 (*NQO1*), sulfiredoxin 1 (*SRXN1*), glutaredoxin (*GLRX*), and ATP binding cassette subfamily C member 1 (*ABCC1*) (Fig. 4A). THS2.2 aerosol also clearly induced this oxidative stress gene expression response program at the 4 h time point. Generally, the response to THS2.2 aerosol exposure was reduced, e.g., by 48% (*GCLM*), 20% (*TXNRD1*), 22% (*NQO1*), 21% (*SRXN1*), 41% (*GLRX*), and 34% (*ABCC1*) for low concentration comparisons of the above-mentioned group of strongly responding genes.

To better quantify this oxidative stress response, we leveraged a previously described oxidative stress causal network model and scored its perturbation based on downstream affected gene expression; all exposure conditions resulted in significant perturbation of this network, but perturbation amplitudes were lower for THS2.2 aerosol than for 3R4F CS exposure (with approximately a 70% reduction in NPA values for THS2.2 *vs.* 3R4F for both matched concentrations) (Fig. 4B). Gene expression data for the 24 h time point after exposure were also investigated in an exploratory manner, with a limited number of replicates ($n = 3$ instead of 9; see above) (Fig. S6B and S6C). We observed that 24 h after the last exposure, the general gene expression response decreased, with few significant gene alterations observed for THS2.2 aerosol-exposed cultures at the matching concentration and a much reduced NPA score.

For the miRNA analysis, we focused on the commonly regulated miRNAs and selected the corresponding mRNA targets as described in the Materials and Methods section. Since miRNAs are known to effect relatively small changes in target mRNA expression, we analyzed only the most significantly regulated target genes, with a FDR $\leq$0.05. To further understand their functional involvement, the group of differentially expressed target genes was used for IPA® Canonical Pathways analysis. Selected cellular functions significantly enriched in the differentially expressed genes are listed in Table S2. IPA® analysis revealed that 13 commonly regulated miRNAs could also have a role in the regulation of different target genes involved in oxidative stress (miRNA target panel and Fig. S6A), such as glutathione peroxidase 4 (*GPX4*), nitric oxide synthase 1 (*NOS1*), gamma-glutamyl hydrolase (*GGH*), and autophagy-related 13 (*ATG13*). In line with the mRNA analysis, the quantitative differences between exposure conditions were also reflected by the oxidative-stress related miRNPA values measuring the induced activities in a candidate integrated miRNA-mRNA network (Fig. 4C and S6A).

We complemented these mRNA and miRNA expression analyses with metabolic profiling, for which we focused on the high 3R4F CS and THS2.2 aerosol concentration 4 h after the third exposure (Fig. 4D–F, Fig. S6D–E, and Fig. S7B). The 4 h time point was chosen to capture the direct effects of CS and THS2.2 aerosol on the metabolome and to allow for comparison with the robust gene expression statistics. 3R4F (High) CS exposure significantly affected several metabolites that directly reflect the oxidative challenge induced by CS (Fig. 4D): Methionine is prone to oxidation and both increased levels of methionine sulfoxide and of N-acetyl-methionine-sulfoxide were observed upon 3R4F CS exposure; 3R4F CS shifted the balance from reduced cysteine to oxidized cysteine (cystine); 2-hydroxy fatty acids have been used previously as oxidative stress markers (Tucci et al., 2013; D'alessandro et al., 2015) and both 2-hydroxypalmitate and 2-hydroxystearate significantly increased upon 3R4F CS exposure. The data also indicated an effect of 3R4F CS exposure on antioxidants: vitamin E (gamma-/beta-tocopherol) and threonate (a vitamin C metabolite) increased and the antioxidant urate decreased in the 3R4F CS group (Ames et al., 1981; Battino et al., 2002). In contrast to 3R4F CS, THS2.2 aerosol exposure showed only limited effects on levels of these metabolites, e.g., a non-significant increase in threonate.

Reduced glutathione (GSH) is a central player in the cellular response to oxidative stress as well as in periodontal diseases (Bains and Bains, 2015). Four hours after 3R4F CS exposure, GSH levels were significantly reduced (Fig. 4E and F, for gene expression see Fig. S6F). Several metabolites interlinked with glutathione were altered by 3R4F CS exposure: we observed depletion of cysteine and glycine, increases in γ-glutamyl amino acids, 5-oxoproline, S-adenosyl homocysteine (SAH), and 2-hydroxybutyrate, and, finally, a decrease in S-adenosyl methionine (SAM) and serine.

Cells exposed to THS2.2 aerosol exhibited only a significant increase in cysteinylglycine and gamma-glutamyl threonine and a decrease in guanidinoacetate, but in contrast to 3R4F CS exposure, were still able to maintain high GSH levels and, for example, showed less depletion of cysteine and glycine (see Fig. 4F and Discussion for details).

3.4. Impact of 3R4F CS and THS2.2 aerosol on xenobiotic metabolism

Among the networks presented in this study, xenobiotic metabolism exhibited a strong perturbation after 3R4F CS exposure and a relatively higher impact of THS2.2 aerosol with respect to the other networks (Fig. 3, NPA panel). We investigated in detail which genes were impacting this network the most. The results shown in the heatmap (Fig. 5A) indicate strong up-regulation at all concentrations for both 3R4F CS and THS2.2 aerosol of the *CYP1A1*/*CYP1B1*, Aldo-keto reductases (*AKR*) *1C1*/*1C2*/*1C3*, TCDD inducible poly(ADP-ribose) polymerase (*TIPARP*), and aryl-hydrocarbon

Fig. 4. Differential induction of oxidative stress by 3R4F CS and THS2.2 aerosol. (**A**) Induction of oxidative stress response program: differential expression heatmap for genes of the reactive oxygen species pathway (HALLMARK_REACTIVE_OXIGEN_SPECIES_PATHWAY; M5938) (Liberzon et al., 2015), as well as for genes and miRNAs belonging to the "Oxidative Stress" candidate miRNA-mRNA network (Fig. S6A). The "*" indicates statistically significant differential expression (FDR <0.05), as explained in the Materials and Methods section. n = 6–9. (**B**) Assessment of exposure effects on the "Oxidative Stress" network. Bars show overall network perturbation amplitudes (NPA scores) based on transcriptomics data. Error bars delimit their 95% confidence intervals. Three statistics are shown: the red star indicates statistical significance with respect to the biological replication (i.e. 95% confidence intervals do not contain the 0 value), while the green and red stars indicate significant specificity statistics with respect to the network structure ("O" and "K" statistics; see the Materials and Methods section). n = 6–9. (**C**) Assessment of exposure effects on the candidate integrated miRNA-mRNA network for oxidative stress based on the miRNomics and transcriptomics data (miRNPA scores). Error bars delimit the 95% confidence intervals (see the Materials and Methods section). n = 6–9. (**D**) Metabolomics profiling was conducted 4 h after exposure of the tissue to high 3R4F CS and THS2.2 aerosol concentrations. Boxplots summarize the response of metabolites sensitive to oxidative stress (blue dots indicate individual samples, n = 5). Significant differences between exposed groups and their respective sham groups are indicated by filled colored boxes and a star ("*" means FDR <0.05). (**E**) Summary of exposure effects on glutathione and related metabolic reactions. Relevant metabolic reactions of the glutathione pathway, including the gamma-glutamyl cycle, cysteine and methionine metabolism, and glycine, serine, and threonine metabolism (Kanehisa et al., 2014). Significantly up- or down-regulated metabolites and genes are marked with red and green, respectively. See Fig. S7 for details on metabolite expression changes. (**F**) Boxplots for metabolites from (E). Note that 2-hydroxybutyrate is isobar with 2-hydroxyisobutyrate.

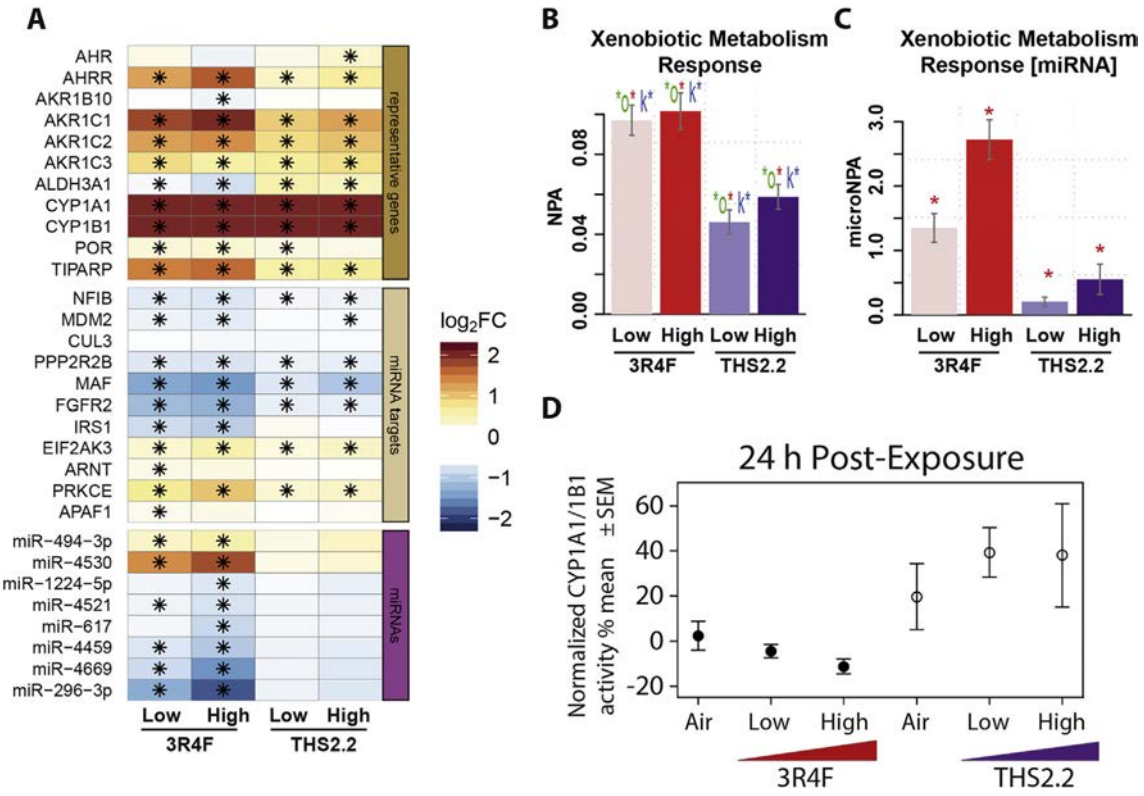

Fig. 5. Xenobiotic metabolism and CYP activity in 3R4F CS- and THS2.2-exposed gingival cultures. (**A**) Heatmap shows differential expression for genes representative of xenobiotic metabolism as well as for genes and miRNAs belonging to the "Xenobiotic Metabolism" candidate miRNA-mRNA network (Fig. S8A). The "*" indicates statistically significant differential expression (FDR <0.05), as explained in the Materials and Methods section. n = 6–9. (**B**) Assessment of exposure effects on the "Xenobiotic Metabolism Response" network. Bars show overall network perturbation amplitudes (NPA scores). Error bars delimit 95% confidence intervals. Statistical significance with respect to three different criteria is indicated by colored stars (see Fig. 4B legend for details). n = 6–9. (**C**) Assessment of exposure effects on the candidate integrated miRNA-mRNA network for "Xenobiotic Metabolism" based on miRNomics and transcriptomics data (miRNPA scores). Error bars delimit 95% confidence intervals (see the Materials and Methods section). n = 6–9. (**D**) Combined activity levels of CYP1A1/CYP1B1 were normalized relative to those in the positive control (TCDD-treated cultures were considered as having 100% activity). Error bars indicate SEM (n = 9). *p < 0.05, compared with the corresponding air control. #p < 0.05, compared with matching concentrations of 3R4F CS.

receptor repressor (*AHRR*) genes.

Biological function analysis of target genes of miRNAs from the IPA® database showed that xenobiotic metabolism was one of the main regulated pathways. The filtering used in IPA® allowed us to connect two up-regulated and six down-regulated miRNAs (Fig. 5A, miRNAs panel, and Fig. S8A) with target genes involved in xenobiotic signaling, such as aryl hydrocarbon receptor nuclear translocator (*ARNT*), nuclear factor I B (*NFIB*), protein kinase C epsilon (*PRKCE*), transcription factor *MAF*, and fibroblast growth factor receptor 2 (*FGFR2*). Interestingly, miRNA were less affected in THS2.2 aerosol-exposed cultures.

The gene expression response at 24 h after the last exposure resulted in an increased impact in 3R4F CS-exposed cultures compared with the 4 h time point, while a general decreased response was recorded for THS2.2 at the low comparable concentration (Fig. S8B). Although the latter results are obtained with a lower number of replicates (n = 3), they indicate that gingival cultures could recover from THS2.2 aerosol exposure while 3R4F CS showed persisting perturbations.

These differences between the exposure conditions were also confirmed for the xenobiotic metabolism-related networks (the actual causal network as well as the candidate integrated miRNA-mRNA network (Fig. S8A)), as illustrated in the bar graphs showing (miR)NPA scores for the different time points (Fig. 5B and C, and Fig. S8C).

We analyzed the combined activity of CYP 1A1 and 1B1 (CYP1A1/1B1), which are involved in phase I metabolism of xenobiotics and whose mRNA was shown to be highly up-regulated by both 3R4F CS and THS2.2 aerosol. These CYPs are of particular importance since they metabolize several toxicants present in CS, such as polycyclic aromatic hydrocarbons, nitrosamines, acrylamines, and nicotine, and they can also be induced in buccal and gingival epithelium *in vivo* and *in vitro* (Vondracek et al., 2001; Schlage et al., 2014). The results in Fig. 5D show that the activity of CYP1A1/1B1 was not altered by 3R4F CS, whereas high rates of activity (~40% of the positive control), although not statistically different from 3R4F CS-exposed cultures, were observed 24 h after the 3-day exposure to THS2.2 aerosol (see Discussion for details).

3.5. Expression and secretion of proinflammatory mediators in 3R4F CS- and THS2.2 aerosol-exposed cultures

We analyzed the expression of inflammatory response genes in gingival cultures exposed to 3R4F CS and THS2.2 aerosol. The heatmap in Fig. 6A shows the inflammation-related gene expression changes measured 4 h after exposure. Among these genes, *IL1A*, *IL1B*, *MMP1*, *MMP3*, *MMP10*, *IL24*, early growth response 1 (*EGR*), connective tissue growth factor (*CTGF*), and prostaglandin-endoperoxide synthase 2 (*PTGS2*) showed considerably high up-regulation following 3R4F CS exposure, whereas only *CXCL14* was found to be severely down-regulated by 3R4F CS. In general, we observed the same regulation patterns in THS2.2-exposed gingival cultures, although to a reduced extent.

We found that 11 of the 3R4F CS and THS2.2 aerosol-regulated

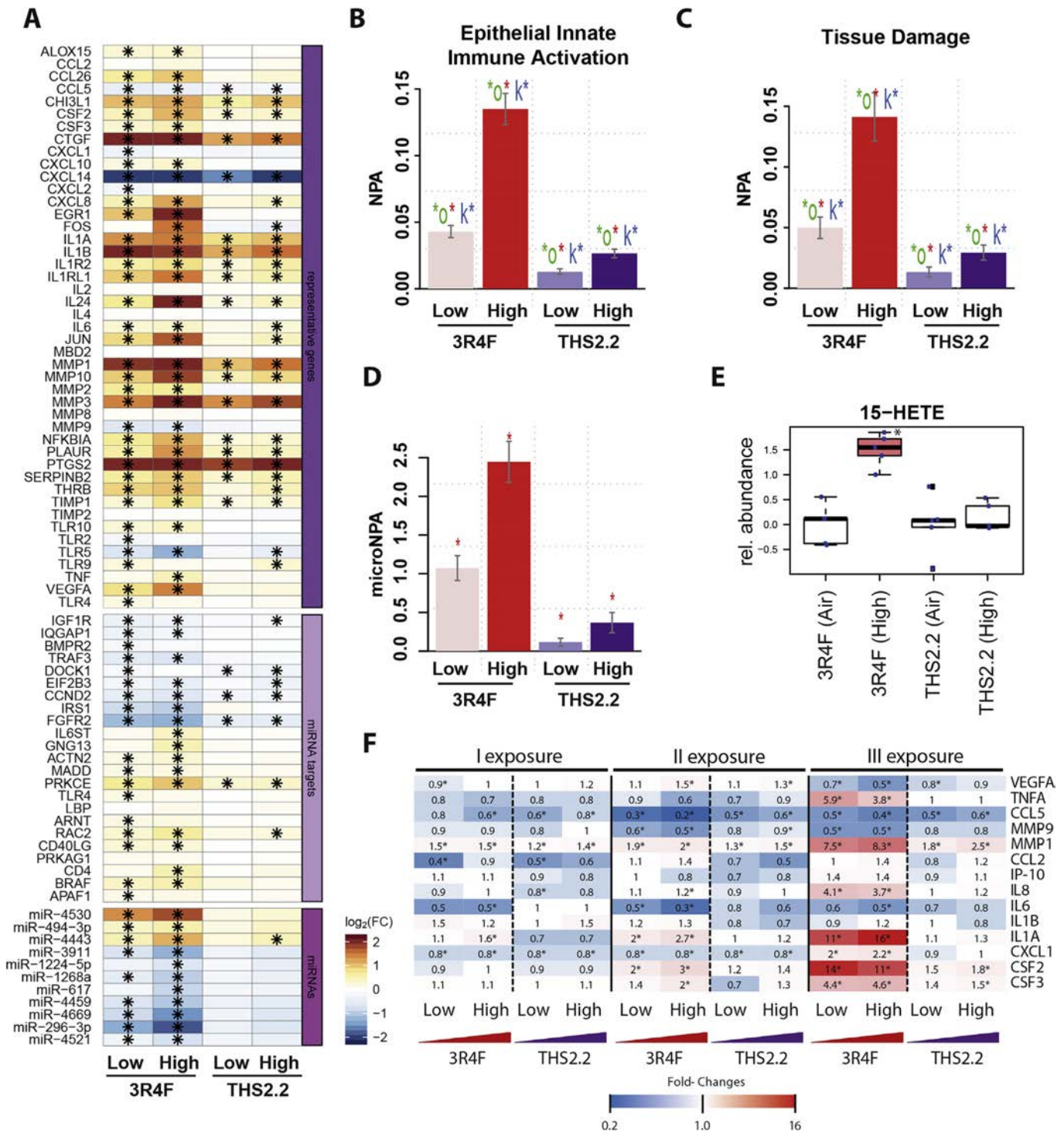

Fig. 6. Profile of inflammation in 3R4F CS- and THS2.2 aerosol-exposed gingival cultures. **A**) Heatmap shows differential expression for genes representative of inflammation as well as for genes and miRNAs belonging to the "Inflammation" candidate miRNA-mRNA network (Fig. S9A). The "*" indicates statistically significant differential expression (FDR <0.05), as explained in the Materials and Methods section. n = 6–9. (**B**–**C**) Assessment of exposure effects on the inflammation networks "Epithelial Innate Immune Activation" and "Tissue Damage". Bars show overall network perturbation amplitudes (NPA scores). Error bars delimit 95% confidence intervals. Statistical significance with respect to three different criteria are indicated by colored stars (see Fig. 4B for details). n = 6–9. (**D**) Assessment of exposure effects on the candidate integrated miRNA-mRNA network for "Inflammation" based on miRNomics and transcriptomics data (miRNPA scores). Error bars delimit 95% confidence intervals (see the Materials and Methods section). n = 6–9. (**E**) Metabolomics profiling was conducted 4 h after exposure of the tissue to high 3R4F CS and THS2.2 aerosol concentrations. Boxplot summarizes the response of 15-HETE (blue dots indicate individual samples, n = 5). Significant differences between exposed groups and their respective sham groups are indicated by filled colored boxes and a star ("*") (FDR <0.05). (**F**) Heatmap showing fold-changes of mean concentrations of proinflammatory mediators in exposed cultures relative to those in their corresponding air controls 24 h after each exposure (I, II, III exposure). Blue and red colors indicate negative or positive fold-changes, respectively, in 3R4F CS- and THS2.2 aerosol-exposed samples compared with air-exposed samples. Nicotine concentrations in smoke or aerosol are indicated for each group (mg/L, x-axis). n = 9.

miRNAs might also have an impact in the inflammatory response (Fig. 6A, miRNA panel, and Fig. S9A). IPA® analysis showed that some of these miRNA-mRNA target genes are associated with cytokine-mediated inflammatory responses: *NFκB*, *IL1*, *IL6*, *IL8* (*CXCL8*), *GMCSF* (*CSF2*), *VEGF*, *CXCR4*, and *TNFR1*. Among these genes, we found interleukin 6 signal transducer (*IL6ST*) (Scheller et al., 2011), toll like receptor 4 (*TLR4*), and CD 40 ligand (*CD40LG*) (Fig. 6A, miRNA targets panel).

In line with the results obtained for oxidative stress and xenobiotic metabolism genes, we also observed a reduction in gene alterations in THS2.2 aerosol-exposed cultures at 24 h post exposure (except for *MMP1* and *MMP10*), whereas in 3R4F CS-exposed counterparts, changes were still greater and, in some cases, exacerbated when compared with the 4 h post exposure (Fig. S9B).

NPA scores for "Epithelial Innate Immune Activation" and "Tissue Damage" networks (Fig. 6B and C, and Fig. S9C and D) as well as miRNPA scores for a candidate integrated miRNA-mRNA network (Fig. 6D) all indicated a concentration-dependent effect in both 3R4F CS and THS2.2 aerosol-exposed cultures, although reduction in the impact was marked for THS2.2 aerosol-exposed cultures.

15-hydroxyeicosatetraenoic acid (15-HETE) is generated by oxidation of arachidonic acid by lipoxygenase 15 (LOX-15) enzymes and has been associated, for example, with immuno-regulatory effects and atherosclerotic processes (Powell and Rokach, 2015; Henriksson et al., 1985; Kundumani-Sridharan et al., 2013; Serhan et al., 2003). Metabolomics analysis performed on the high 3R4F CS and THS2.2 aerosol concentrations 4 h after the last exposure showed a significant increase in the regulation of 15-HETE by 3R4F CS but not by THS2.2 aerosol (Fig. 6E).

Fig. 6F illustrates the secretion of different proinflammatory mediators over the three exposures to 3R4F CS and THS2.2 aerosol (see Materials and Methods for the sampling procedure). In general, major changes were observed in the proinflammatory mediators that accumulated in media for 24 h after the last exposure to 3R4F CS (see also Fig. S10); the secretion of different proinflammatory mediators (MMP-1, IL-8, IL-1A, CSF2, and CSF3) increased slightly with respect to the air control after the second CS exposure but became markedly higher after the third (TNFA, MMP-1, CXCL1, IL-8, IL-1A, CSF2, and CSF3), with values reaching 16-fold of the control (IL-1A). VEGFA, CCL5, MMP-9, and IL-6 were down-regulated after 3R4F CS exposure. In contrast with what was observed for the increased secretion of the inflammatory mediators, mostly observable after the third exposure, inhibition of secretion of these markers did not follow a trend, leading to mixed responses over the exposure period.

There was not always a clear dose-dependency in the amplitude of the release; this might be due to the damage observed at the high 3R4F CS concentration, which might indicate a reduced number of viable cells and/or an impairment in the capability of the cells to secrete inflammatory mediators.

Responses of gingival cultures exposed to THS2.2 aerosol were milder or none, with the same trend of release observable for a few proinflammatory markers (CSF2, CSF3, CCL5, MMP-1), although to a much lower level than observed in 3R4F CS-exposed counterparts.

3.6. Keratinization and cell–cell adhesion upon 3R4F CS and THS2.2 aerosol exposure

Overt keratinization of gingival cultures was observed after exposure to 3R4F CS, in particular, after exposure to the high concentration. Hyperkeratinization of oral epithelia can occur in response to chemical inducers, like CS (Gualerzi et al., 2012; Orellana-bustos et al., 2004), and keratohyalin granules are often an indication of keratinizing epithelia (Muller and Schroeder, 1980; Plackova and Skach, 1975; Singh et al., 1979).

Fig. 7A illustrates that, 24 h after three repeated exposures to 3R4F CS at the low concentration, hypergranulosis with coarse keratohyalin granules spreading both in the stratum granulosum and the stratum corneum (arrows) was present. The high 3R4F CS concentration showed complete keratinization of the epithelium, extending until the membrane, along with overt parakeratosis (arrows). THS2.2 aerosol-exposed cultures also showed the presence of keratohyalin granules at both high and low concentrations, although hyperkeratinization of the epithelial cells was not detected.

Fig. 7B shows the expression profiles for genes, measured 4 h after repeated exposures, that were reported as markers of normal oral epithelial differentiation or previously described in non-neoplastic lesions and in reconstituted *in vitro* tissues (Donetti et al., 2010; Kimball et al., 2006; Su et al., 1993; Yoshizawa et al., 2012; Bloor et al., 1998; Mahoney et al., 2006; Mirowsk et al., 1996; Kose et al., 2007). The majority of the represented keratin (*KRT*) genes were down-regulated with exposure to 3R4F CS, with almost no difference between low and high concentrations (*KRT1, 5*, *10*, *13*, *14*, *15*, *19*). Among the *KRT* genes analyzed, only *KRT2*, *17*, *76* were up-regulated. mRNAs of the keratinization-related genes involucrin (*IVL*) and filaggrin (*FLG*) were up-regulated differentially with low and high 3R4F CS concentrations. *MKI67*, a marker of cell cycle activation, and proliferating cell nuclear antigen (*PCNA*), were both found to be significantly down-regulated. *MAPK14,* defensin beta 1 (*DEFB1*), and pleckstrin homology like domain family a member 1 (*PHLDA1*) were up-regulated in both 3R4F CS-exposed and THS2.2 aerosol-exposed samples. The overall impact of THS2.2 aerosol was reduced compared with 3R4F CS-exposed cultures.

We performed staining at 24 h after the last exposure with an antibody for E-cadherin, a well-studied adhesion molecule in epithelial tissues with important functions in cell–cell adhesion and cell signaling (van Roy and Berx, 2008; Tsang et al., 2012). The pictures in Fig. 7C show that E-cadherin abundance was highly reduced by 3R4F CS exposure, proportionally to the CS concentration applied. THS2.2 aerosol was found to slightly reduce E-cadherin expression only at the high concentration.

We investigated the expression of some representative genes involved in cell adhesion and junction formation after 4 h from the last exposure (Fig. 7D). In agreement with what was observed for E-cadherin staining, we observed that *CDH1*, the gene encoding E-cadherin, was significantly down-regulated by 3R4F CS. The expression of other cadherins was, however, not unequivocal; only *CDH3* was down-regulated, while *CDH2, 4, 5* were all up-regulated. Overall, the cell adhesion genes were mostly down-regulated by 3R4F CS with the exception of *PVRL2* and the more general regulators *MAPK8*, and *JUN*. The heatmap representing tight junction-related genes (Fig. 7E) showed general up-regulation, with only claudin 1 (*CLDN1*) and F11 receptor (*F11R*) exhibiting reduced expression upon 3R4F CS exposure.

The fewer THS2.2 aerosol-induced alterations, where present, were reduced with respect to the corresponding 3R4F CS counterparts.

We also measured gene expression changes at 24 h after the last exposure (Fig. S11). The heatmap shows that there was no significant alteration in gene expression, except for sporadic cases in 3R4F CS-exposed samples (*PHLDA1*, *PCNA*, desmocollin (*DSC*) *1*, *DSC3*, *NOTCH3*, and *CLDN4*) and for only two genes upon high THS2.2 aerosol exposure (*KRT13* and *DCS1*).

4. Discussion

In the present study, we investigated and compared the impact of the aerosol from the candidate MRTP, THS2.2, with that of CS, on

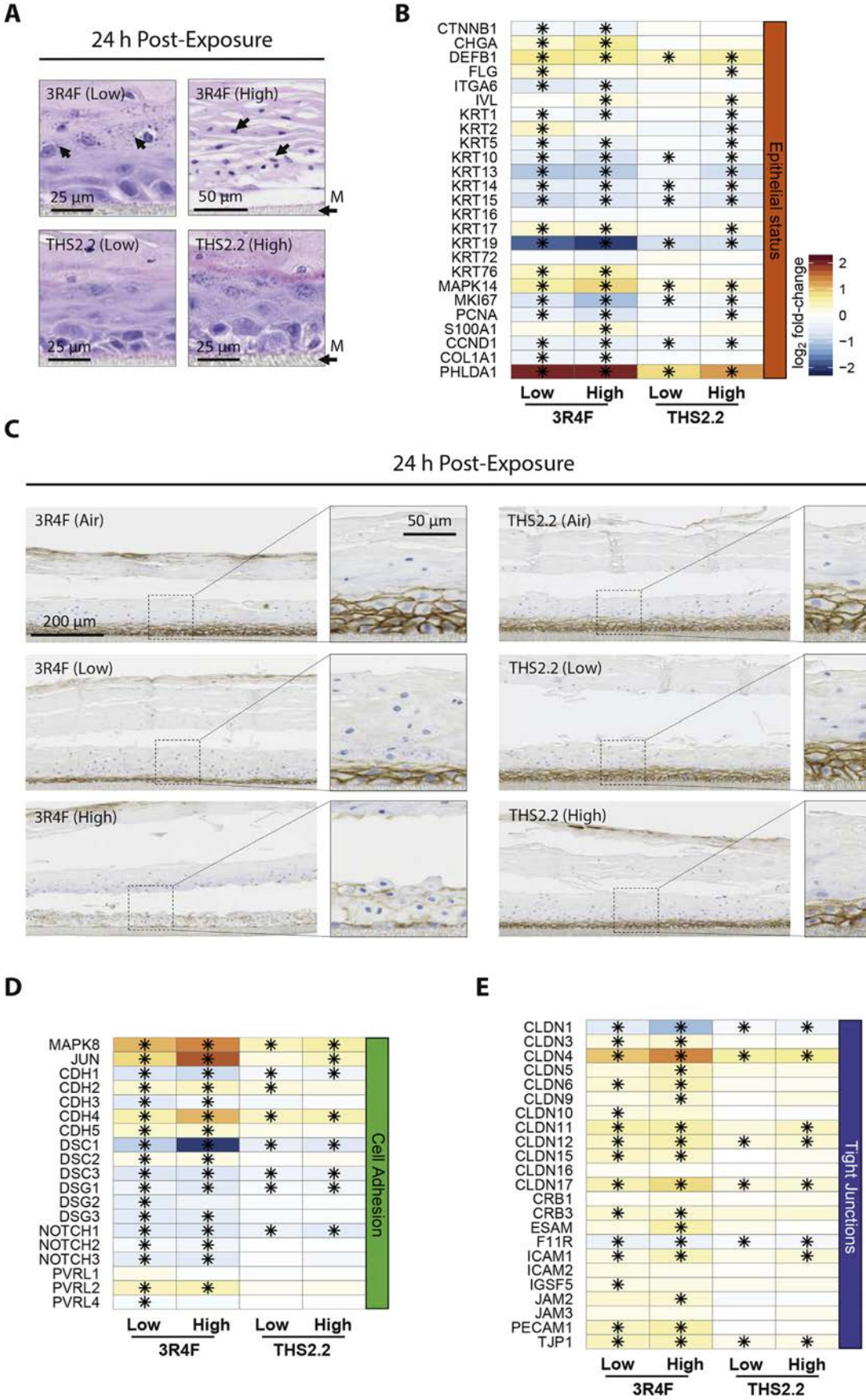

Fig. 7. Keratinization and cell–cell adhesion in 3R4F CS- and THS2.2 aerosol-exposed samples. (**A**) Representative images of H&E-stained gingival culture sections observed 24 h after the last exposure. Staining was performed as described in the Materials and Methods section. Arrows indicate keratohyalin granules (upper left picture) or parakeratosis (upper right picture). Abbreviations: M, membrane. 63 × and 100 × magnification. n = 9. (**B**, **D**, **E**) Heatmaps showing differential expression of genes related to epithelial status/cell type, cell adhesion, or tight junctions. Statistical significance (FDR <0.05) is indicated by a star ("*"), as explained in the Materials and Methods section. n = 6–9. (**C**) Representative images of E-cadherin-stained gingival culture sections observed 24 h after the last exposure. Staining was performed as described in the Materials and Methods section. Magnification is set at 20 × and 63 × for the insets. n = 9.

human gingival epithelial organotypic cultures. The employed EpiGingival™ model reproduces aspects relevant to periodontal diseases, fulfils the 3Rs principle (replacement, reduction, and refinement), and is in line with 21st century toxicology approaches (see introduction) (Balls, 2010; Sheldon and Cohen Hubal, 2009; Berg et al., 2011; Rovida et al., 2015).

4.1. Exposure design

To allow for a physiologically relevant comparison between CS and THS2.2 aerosol, concentrations were matched by delivered dose of nicotine (see methods). To mimic the moistening of gingival mucosa in the oral cavity, the gingival cultures were wetted with PBS on the apical side during the experiments. PBS has a similar composition as artificial saliva, but does not contain the commonly included biological additives (Moharamzadeh et al., 2009). Many different types of artificial saliva with greatly varying compositions are available, of which some do not meet the biophysical properties of real saliva and even induce an inflammatory response in some cell types (Malpass et al., 2013; Kho, 2014; Preetha and Banerjee, 2005).

The deposited nicotine concentrations in PBS for the selected aerosol/CS concentrations (50–100 μg/mL) are 2 orders of magnitude higher than what is observed in human saliva (Jacob et al., 2015; Yuki et al., 2013). However, rapid equilibration with the culture medium likely results in an approx. 10-fold dilution and the measurements for human saliva might – due to rapid equilibration against the blood flow—underestimate the peak concentrations that hit the gingiva during each puff (Yuki et al., 2013). In sum, the applied exposure concentrations in the Vitrocell system are likely to represent the upper range (or above) when compared to the *in vivo* exposure, and higher concentrations are standard for toxicological testing.

4.2. Effects on keratinization

As reported for native gingival epithelium, the gingival cultures underwent extensive hyperkeratinization in response to CS, which extended into deeper layers, such as the stratum spinosum (Villar and Lima, 2003; Shetty and Gokul, 2012; Shirani et al., 2014). This morphological alteration was evidenced by the accumulation of nuclei in the stratum corneum (parakeratinization), which indicates a lack of balance between keratinization and proliferation and is associated with inflammatory infiltrates (Andreescu et al., 2013).

CS-mediated keratinization was further supported by increased gene expression of crosslinking proteins, such as *FLG* and *IVL*, which are expressed in keratohyaline granules in keratinizing tissues (Shetty and Gokul, 2012; Toulza et al., 2007; Candi et al., 2005; Henry et al., 2012; Koster and Roop, 2007). In contrast, other genes involved in keratinization, such as several keratin family members (*KRT13*, *KRT19*), were down-regulated. As terminal cellular differentiation can further decouple mRNA and protein levels, in future studies, protein expression and localization analysis of these markers might help to elucidate the cellular and molecular basis of these changes. Importantly, supporting the translatability potential of our model, the observed down-regulation of certain keratin genes is consistent with previous studies (Donetti et al., 2010; Alharbi and Rouabhia, 2016).

4.3. Effects on cellular adhesion

Down-regulation of E-cadherin (*CDH1*) protein/mRNA and of other cell adhesion-related mRNAs (*DSC1*, *3*, *DSG1*, *2*, *3*) indicated an effect of CS on cellular adhesion processes. These data are in line with previously published results showing that exposure to CS disturbs the gingival epithelial structure, resulting in significant tissue desquamation, particularly with longer exposure periods (Semlali et al., 2011). Down-regulation of E-cadherin by CS in oral mucosa cells has been found in previous studies (Hasegawa et al., 2002; Coppe et al., 2008) and has been associated with tissue dysfunction similar to that in cancer and periodontal diseases (Hirohashi and Kanai, 2003; Arun et al., 2010). In our study, expression of N-cadherin (*CDH2*) was up-regulated, which overall indicates an epithelial to mesenchymal shift in the epithelium (*CDH1* down-regulated, *CDH2* up-regulated) upon CS exposure (Huang et al., 2013).

Further supporting an effect on cellular adhesion, tight junction-related genes were mostly up-regulated upon CS exposure – except *CLDN1*, whose depletion has been linked to hyperkeratosis in mice (Morita et al., 2011; Zhou et al., 2013; Furuse et al., 2002) and which was found to be decreased in human biopsies from patients with periodontitis (Ye et al., 2000). Our previous study, focused on buccal organotypic cultures exposed to CS and THS2.2 aerosol (Zanetti et al., 2016), reported similar results, which indicates a common response of oral tissues despite the different exposure regimen applied (acute *vs.* repeated exposures).

4.4. Activation of cellular response programs

Our multi-omics approach (mRNA, miRNA, and metabolite analysis) showed perturbation of three biological processes that are commonly perturbed by CS exposure and periodontal diseases (Guentsch et al., 2008; Giannopoulou et al., 2003a; Babu et al., 2013; Conard et al., 1975): oxidative stress, xenobiotic metabolism, and inflammation. These three response programs were also highly impacted in previous studies, in which ourselves and others found that CS exposure led to several changes in these core processes in buccal and gingival organotypic cultures (Zanetti et al., 2016; Kirkham and Barnes, 2013; Iskandar et al., 2013; Goldkorn et al., 2014; Schlage et al., 2014).

4.4.1. Oxidative stress

Both CS and THS2.2 aerosol affected the expression of genes involved in the reactive oxygen species pathway – with only a slightly reduced effect for THS2.2 aerosol compared with CS at the 4 h post exposure time point. However, the quantified impact at the causal oxidative stress network level, which represents a prediction of the activity state of this process, was much reduced for THS2.2 aerosol-exposed cultures. This difference in the (predicted) activation state of the oxidative stress response was supported by metabolomics data, which clearly showed a reduced perturbation of metabolites by THS2.2 aerosol than CS, especially for the glutathione pathway.

Reduced glutathione is a pivotal player in periodontal diseases (Bains and Bains, 2015). The observed concomitant depletion of cysteine and glycine, two of the building blocks for glutathione, after CS exposure likely indicate the (insufficient) attempt of the cells to regenerate glutathione. The increase in the glutathione regeneration pathway (increases in γ-glutamyl amino acids and the pathway intermediate 5-oxoproline) (Inoue, 2016) and in the SAM cycle and the transsulfuration pathway (Beatty and Reed, 1980; Mosharov et al., 2000) (e.g., increase in SAH and 2-hydroxybutyrate; decrease in SAM and serine) might indicate an attempt to restore the levels of cysteine and glycine to replenish glutathione levels.

In contrast to 3R4F CS exposure, cells exposed to THS2.2 aerosol were still able to maintain high glutathione levels. This effect is likely ascribable to the lower oxidative challenge of THS2.2 aerosol compared with 3R4F CS. In addition, gene expression

measurements at the 24 h time point showed that the response to THS2.2 aerosol diminished with post exposure duration, indicating that the cells can more easily cope with the reduced oxidative challenge of THS2.2 aerosol than CS.

IPA® analysis suggested that 13 commonly regulated miRNAs might also play a role in the regulation of important pathways related to oxidative stress in the context of gingival pathologies, such as: NRF2-mediated oxidative stress (Tamaki et al., 2014), glutathione redox reactions I, glutathione-mediated detoxification, both important antioxidant mechanisms in the periodontitis (Bains and Bains, 2015), and HMGB1 signaling, which is activated by oxidative stress and is involved in inflammation and cell death (YU et al., 2015; Luo et al., 2011; Nogueira et al., 2014). Notably, the majority of the miRNAs and their corresponding target genes were less impacted by THS2.2 aerosol.

4.4.2. Xenobiotic metabolism

Xenobiotic metabolism represents the first line of defense against inhaled toxicants (Omiecinski et al., 2011) and was the most clearly impacted network by CS exposure according to NPA analysis and IPA® investigation. Overall gene expression at 4 h after repeated exposures showed marked differences between 3R4F CS-exposed cultures and THS2.2 aerosol-exposed cultures. The NPA score was much lower for THS2.2 aerosol-exposed cultures for both miRNA and mRNA subsets of data. IPA® analysis on the miRNA dataset confirmed lower alterations in common miRNAs and gene targets in cultures exposed to THS2.2 aerosol. Among the predicted genes modulated by miRNAs, we found *ARNT*, required for the proper functioning of the aryl hydrocarbon receptor and a mediator of xenobiotic toxicity (Monnouchi et al., 2016), and *NFIB*, which binds to the ARNT complex (Ingenuity® database).

Exploratory analysis at 24 h post-exposure indicated a recovery trend for THS2.2 aerosol-exposed cultures. Analysis at later post exposure time points could have better highlighted the different recovery potential of cells exposed to 3R4F CS and THS2.2 aerosol, as already shown in our previous work (Zanetti et al., 2016).

THS2.2 aerosol-exposed cultures exhibited a higher CYP1A1/1B1 enzyme activity than 3R4F CS, in spite of similarly high induction of gene expression. The differential activity of this CYP has already been observed in our previous study and an extensive discussion has been provided on this result (Zanetti et al., 2016). One of the possibilities is that metal-induced heme oxygenase potently inhibited CYP1A1 enzyme activity, as it is reported for TCDD-induced CYP1A1 in human and rat hepatocytes (Amara et al., 2010; Anwar-mohamed et al., 2012; Korashy and El-Kadi, 2012). Interestingly, in our results, the heme oxygenase 1 (*HMOX1*) gene was up-regulated by CS (1.39 and 1.86 folds for low and high 3R4F CS respectively, data not shown) and decreased by THS2.2 aerosol (0.51 and 0.77 for low and high THS2.2 CS respectively, data not shown) at 4 h post exposure. Moreover, other prototypic heat-not-burn products are reported to induce *CYP1A1* expression in rat lungs (Kogel et al., 2014), as did an aerosol of nicotine in PBS (Phillips et al., 2015). Further studies are needed to clarify the mechanism behind THS2.2 aerosol-mediated activation of CYP.

4.4.3. Inflammation

Inflammation is one of the pivotal processes in the context of periodontal diseases (Giannopoulou et al., 2003a; Guentsch et al., 2008). CS exposure resulted in a significant higher impact on proinflammatory mediators than THS2.2 aerosol exposure, with peak alterations 24 h after the last exposure session.

IL-8 secretion was significantly up-regulated by CS. Exacerbation of IL-8 secretion has been shown in a model of bacterial infection employing human gingival epithelial cells exposed to CS extract (Mahanonda et al., 2009) and increased levels of IL-8 were found in gingival crevicular fluid of smokers (Giannopoulou et al., 2003a, 2003b).

Up-regulated expression of *MMP1*, 2, *3*, *10* was measured along with increased expression, although to a lower fold-change, of MMP inhibitor *TIMP1*, but not *TIMP2*. MMPs are important players in periodontitis, in which their main role is in matrix degradation (Popat et al., 2014; Sapna et al., 2014) and they can be activated by CS in gingival tissues (Ozcaka et al., 2011). Luminex-based analysis revealed strong up-regulation by 3R4F CS of MMP-1 and down-regulation of MMP-9. MMP-1 has been proposed as a potential marker of tissue repair in periodontitis patients because of its function in tissue remodeling (Romanelli et al., 1999), and it was found to be increased in oral inflammatory models (Kim et al., 2006). MMP-9 is mostly secreted by fibroblasts, which might explain the discrepancy in the high levels of MMP-9 observed in smokers (Ozcaka et al., 2011). In our previous study on CS-exposed organotypic gingival cultures, only VEGF and MMP-1 secretion were increased and MMP-9 and IP-10 were decreased (Schlage et al., 2014); this limited response could be due to the presence of fibroblasts and a single-day exposure.

Secretion of CSF2 (also named GM-CSF), TNFA, and IL-1A was also strongly increased by CS. Stimulation of CSF2 production by gingival keratinocytes might cause accumulation and activation of neutrophils in the epithelium and could contribute to the initiation and development of inflammation in periodontal tissues (Sugiyama et al., 2002). TNFA levels have been reported to be up-regulated in gingival tissues of smokers (Bostrom et al., 1998, 1999; Ojima and Hanioka, 2010). IL-1A (together with IL-1B) may have multiple adverse effects on periodontal tissues including increased bone resorption, increased collagen turnover, and stimulation of other inflammatory cytokines (De Nardin, 2001). In contrast, THS2.2 aerosol exerted only a weak response for MMP-1 and CSF2 and 3 and an attenuated gene expression profile modulation compared to CS.

IPA® analysis suggested that some miRNA target genes could be associated, predominantly upon CS exposure, with the inflammatory response. Among these genes, we found *IL6ST*, which is important for IL-6 signaling (Scheller et al., 2011), *TLR4*, which enhances inflammatory cytokine production in gingival tissue (Eskan et al., 2008), and *CD40LG*, whose activation leads to secretion of cytokines by epithelial cells (Dallman et al., 2003).

Metabolomics showed that the lipid mediator 15-HETE was up-regulated by 3R4F CS but not THS2.2 aerosol. 15-HETE is generated by oxidation of arachidonic acid by the enzyme ALOX-15 and is associated with immuno-regulatory effects and atherosclerotic processes (Powell and Rokach, 2015; Henriksson et al., 1985; Kundumani-Sridharan et al., 2013; Serhan et al., 2003). Overexpressed activity of ALOX-15 has been associated with bone loss and inflammation in a rabbit model of periodontitis (Serhan et al., 2003). Interestingly, mRNA expression of *ALOX-15* was up-regulated in our experimental model after CS exposure but not THS2.2 aerosol.

4.5. Study limitations

The employed organotypic culture system represents the gingival epithelium formed by keratinocytes. Other cell types relevant to the pathogenesis of periodontal diseases (Di Benedetto et al., 2013), notably fibroblasts in the periodontal soft connective tissue and immune-cells were not included in our model. Thus, our model is focused on the initial mechanisms centered on the epithelium. As, for example, shown in our previous publication (Schlage et al., 2014), these cultures can be further complemented by additional cell types, including fibroblasts. Especially, in a study with an extended repetitive exposure regime, such a more complex

tissue culture system could yield further insights into the role of regulatory interactions between different cell types in the CS exposure response – however, such a multi cell type system would also make the assignment of transcriptome and metabolome effects to specific cell types more challenging. Also, as discussed for the observed downregulation of several keratin family members (*KRT13*, *KRT19*), tight coupling of mRNA and protein levels cannot always be expected. Thus, future studies could benefit from more extensive protein expression measurements. Similarly, to further our understanding on how the observed gene expression changes relate to the tissue architecture, more extensive protein/gene localization studies could be performed. In addition, in the current study design we mostly focused on the early exposure effects (4 h) for the transcriptomics and metabolomics analyses. This did not allow us to fully compare the recovery potential of the observed effects over time. Finally, multiple donors would be helpful to further confirm these results.

5. Conclusions

In this study, we provide a large body of results highlighting a reduced impact for the candidate MRTP, THS2.2, compared with 3R4F CS on human gingival epithelial organotypic cultures. We observed no cytotoxicity, and reduced impact on the release of proinflammatory mediators and on the pathophysiology of the gingival cultures after repeated THS2.2 aerosol exposure compared with CS. Computational analysis of transcriptomics data also supported a general lower effect of THS2.2 aerosol on mRNA and miRNA levels – with possible correlations between miRNAs and putative target genes –for the “oxidative stress”, “xenobiotic metabolism” and “inflammation” networks. The 4 h post-exposure response of the transcriptome to THS2.2 aerosol was not only lower than for 3R4F CS, but also more transient as evaluated by the transcriptome response 24 h after exposure. This result is consistent with our previous investigations with buccal (Zanetti et al., 2016) and nasal organotypic cell culture models (Iskandar et al., 2016).

Taken together, this study indicates that exposure to THS2.2 aerosol had no obvious acute toxicity and a lower impact on the pathophysiology of human gingival organotypic cultures. The effects of CS on gingival cultures mirrored several pathophysiological conditions and molecular changes observed in the native gingival mucosa of smokers, making this model a potential tool for preclinical predictive *in vitro* research.

Conflicts of interest statement

All authors are employees of, or (W. K. Schlage) contracted and paid by Philip Morris International., except Brian R. Keppler (Metabolon Inc.).

Funding sources

Philip Morris International is the sole source of funding and sponsor of this project.

Acknowledgements

The authors acknowledge the technical expertise of David Bornand, Rémi Dulize, Dariusz Peric, and Karine Baumer for RNA sample processing and transcriptomics data generation. We would like to thank Sam Ansari for his support in the biobanking recording of samples. We thank Céline Merg and Maica Corciulo for the proinflammatory mediator measurements. We also acknowledge the technical expertise of Abdelkader Benyagoub, Camille Schilt, and Maude Mayer for histological processing. We thank Quentin Dutertre, Mounir Rhouma and Arno Knorr for the nicotine assessment experiments. We also thank Dr. Mark Wilsher for histopathological analysis of the organotypic culture model.

Abbreviations

3Rs	replacement, reduction, and refinement
15-HETE	15-hydroxyeicosatetraenoic acid
AK	adenylate kinase
ALOX/LOXE	lipoxygenase
BIF	biological impact factor
CCL	chemokine (C-C motif) ligand
CEE	6'-chloroethyl ether
CFA	cell fate and angiogenesis
CPR	cell proliferation
CS	cigarette smoke
CSF	colony stimulating factor
CST	cellular stress
CXCL	chemokine (C-X-C motif) ligand
CYP	cytochrome P450
DE	differentially expressed gene
DRF	dose range finding
ESI	electrospray ionization
FDR	false discovery rate
GSA	gene set analysis
GSH	reduced glutathione
HBD	human beta defensing
H&E	hematoxylin and eosin
IL	interleukin
IP	Interferon gamma-induced protein
IPN	inflammatory process network
IPA	Ingenuity® Pathway Analysis
ISO	international organization for standardization
KEGG	Kyoto encyclopedia of genes and genomes
LC	liquid chromatography
M	membrane
MAP	multi-analyte profiling
mirDE	differentially expressed miRNA
miRNA	micro RNA
MMP	matrix metalloproteinase
MRTP	modified risk tobacco product
MS	mass spectrometry; N, number
NPA	network perturbation amplitude
NRF	Nuclear factor (erythroid-derived 2)-like
PBS	phosphate-buffered saline
PMI	Philip Morris International
QC	quality control
RP	reverse phase
SAH	S-adenosyl homocysteine
SAM	S-adenosyl methionine;
SB	stratum basale
SC	stratum corneum
SEM	standard error of the mean
SG	stratum granulosum
SM	smoking machine
SS	stratum spinosum
TCDD	2,3,7,8-tetrachlorodibenzodioxin
THS	tobacco heating system
TNF	tumor necrosis factor
UP	ultra performance
w/v	weight/volume
VEGFA	vascular endothelial growth factor alpha

Transparency document

Transparency document related to this article can be found online at http://dx.doi.org/10.1016/j.fct.2016.12.027.

Appendix A. Supplementary data

Supplementary data related to this article can be found at http://dx.doi.org/10.1016/j.fct.2016.12.027.

References

Agrawal, A., Shindell, E., Jordan, F., Baeva, L., Pfefer, J., Godar, D.E., 2013. UV radiation increases carcinogenic risks for oral tissues compared to skin. Photochem Photobiol. 89, 1193–1198.

Van roy, F., Berx, G., 2008. The cell-cell adhesion molecule E-cadherin. Cell Mol. Life Sci. 65, 3756–3788.

Alharbi, I.A., Rouabhia, M., 2016. Repeated exposure to whole cigarette smoke promotes primary human gingival epithelial cell growth and modulates keratin expression. J. Periodontal Res. 51, 630–638.

Amara, I.E., Anwar-mohamed, A., El-kadi, A.O., 2010. Mercury modulates the CYP1A1 at transcriptional and posttranslational levels in human hepatoma HepG2 cells. Toxicol. Lett. 199, 225–233.

Ames, B.N., Cathcart, R., Schwiers, E., Hochstein, P., 1981. Uric acid provides an antioxidant defense in humans against oxidant- and radical-caused aging and cancer: a hypothesis. Proc. Natl. Acad. Sci. U. S. A. 78, 6858–6862.

Andreescu, C.F., mihai, L.L., Raescu, M., Tuculina, M.J., Cumpata, C.N., Ghergic, D.L., 2013. Age influence on periodontal tissues: a histological study. Rom. J. Morphol. Embryol. 54, 811–815.

Anwar-mohamed, A., Klotz, L.O., El-kadi, A.O., 2012. Inhibition of heme oxygenase-1 partially reverses the arsenite-mediated decrease of CYP1A1, CYP1A2, CYP3A23, and CYP3A2 catalytic activity in isolated rat hepatocytes. Drug Metab. Dispos. 40, 504–514.

Arun, R., Hemalatha, R., Arun, K.V., Kumar, T., 2010. E-cadherin and CD1a expression in gingival epithelium in periodontal health, disease and post-treatment. Indian J. Dent. Res. 21, 396–401.

Babu, S.P., Ramesh, V., Samidorai, A., Charles, N.S., 2013. Cytochrome P450 2C9 gene polymorphism in phenytoin induced gingival enlargement: a case report. J. Pharm. Bioallied Sci. 5, 237–239.

Bains, V.K., Bains, R., 2015. The antioxidant master glutathione and periodontal health. Dent. Res. J. (Isfahan) 12, 389–405.

Balls, M., 2010. Atla (alternatives to laboratory animals): past, present and future. Altern. Lab. Anim. 38, 437–441.

Battino, M., Ferreiro, M., Gallardo, I., Newman, H., Bullon, P., 2002. The antioxidant capacity of saliva. J. Clin. Periodontology 29, 189–194.

Beatty, P.W., Reed, D.J., 1980. Involvement of the cystathionine pathway in the biosynthesis of glutathione by isolated rat hepatocytes. Archives Biochem. Biophysics 204, 80–87.

Berg, N., De wever, B., Fuchs, H.W., Gaca, M., Krul, C., Roggen, E.L., 2011. Toxicology in the 21st century–working our way towards a visionary reality. Toxicol Vitro 25, 874–881.

Bergstrom, J., 2004. Tobacco smoking and chronic destructive periodontal disease. Odontology 92, 1–8.

Bloor, B.K., Su, L., Shirlaw, P.J., Morgan, P.R., 1998. Gene expression of differentiation-specific keratins (4/13 and 1/10) in normal human buccal mucosa. Lab. Invest. 78, 787–795.

Bostrom, L., Linder, L.E., Bergstrom, J., 1998. Clinical expression of TNF-alpha in smoking-associated periodontal disease. J. Clin. Periodontol. 25, 767–773.

Bostrom, L., Linder, L.E., Bergstrom, J., 1999. Smoking and crevicular fluid levels of IL-6 and TNF-alpha in periodontal disease. J. Clin. Periodontol. 26, 352–357.

Boue, S., Talikka, M., Westra, J.W., Hayes, W., Di fabio, A., Park, J., Schlage, W.K., SEwer, A., Fields, B., Ansari, S., Martin, F., Veljkovic, E., Kenney, R., Peitsch, M.C., Hoeng, J., 2015. Causal biological network database: a comprehensive platform of causal biological network models focused on the pulmonary and vascular systems. Database (Oxford), 2015, bav030.

Candi, E., Schmidt, R., Melino, G., 2005. The cornified envelope: a model of cell death in the skin. Nat. Rev. Mol. Cell Biol. 6, 328–340.

Carnevali, S., Petruzzelli, S., Longoni, B., Vanacore, R., Barale, R., Cipollini, M., Scatena, F., PAggiaro, P., Celi, A., Giuntini, C., 2003. Cigarette smoke extract induces oxidative stress and apoptosis in human lung fibroblasts. Am. J. Physiol. Lung Cell Mol. Physiol. 284, L955–L963.

Chapple, I.L., Milward, M.R., Dietrich, T., 2007. The prevalence of inflammatory periodontitis is negatively associated with serum antioxidant concentrations. J. Nutr. 137, 657–664.

Conard, G.J., Osborn, J.C., Pekary, A.D., Scholle, R.H., 1975. Relationship of drug metabolism and inflammation to the gingival response of rats treated with diphenylhydantoin. J. Dent. Res. 54 (Spec No B), B68–B74.

Coppe, J.P., Boysen, M., Sun, C.H., Wong, B.J., Kang, M.K., Park, N.H., Desprez, P.Y., Campisi, J., Krtolica, A., 2008. A role for fibroblasts in mediating the effects of tobacco-induced epithelial cell growth and invasion. Mol. Cancer Res. 6, 1085–1098.

D'aiuto, F., Nibali, L., Parkar, M., Patel, K., Suvan, J., Donos, N., 2010. Oxidative stress, systemic inflammation, and severe periodontitis. J. Dent. Res. 89, 1241–1246.

D'alessandro, A., Hansen, K., Silliman, C., Moore, E., Kelher, M., Banerjee, A., 2015. Metabolomics of AS-5 RBC supernatants following routine storage. Vox Sang. 108, 131–140.

Dallman, C., Johnson, P.W., Packham, G., 2003. Differential regulation of cell survival by CD40. Apoptosis 8, 45–53.

Davis, M.A., Eldridge, S., Louden, C., 2013. Chapter 10-biomarkers: discovery, qualification and application. In: Wallig, W.M.H.G.R.A. (Ed.), Haschek and Rousseaux's Handbook of Toxicologic Pathology, third ed. Academic Press, Boston.

De Nardin, E., 2001. The role of inflammatory and immunological mediators in periodontitis and cardiovascular disease. Ann. Periodontol. 6, 30–40.

Di Benedetto, A., Gigante, I., Colucci, S., Grano, M., 2013. Periodontal disease: linking the primary inflammation to bone loss. Clin. Dev. Immunol. 2013.

Donetti, E., Gualerzi, A., Bedoni, M., Volpari, T., Sciarabba, M., Tartaglia, G., Sforza, C., 2010. Desmoglein 3 and keratin 10 expressions are reduced by chronic exposure to cigarette smoke in human keratinised oral mucosa explants. Arch. Oral Biol. 55, 815–823.

Eskan, M.A., Rose, B.G., Benakanakere, M.R., Zeng, Q., Fujioka, D., Martin, M.H., Lee, M.J., Kinane, D.F., 2008. TLR4 and S1P receptors cooperate to enhance inflammatory cytokine production in human gingival epithelial cells. Eur. J. Immunol. 38, 1138–1147.

Evans, A.M., Dehaven, C.D., Barrett, T., Mitchell, M., Mllgram, E., 2009. Integrated, nontargeted ultrahigh performance liquid chromatography/electrospray ionization tandem mass spectrometry platform for the identification and relative quantification of the small-molecule complement of biological systems. Anal. Chem. 81, 6656–6667.

Family Smoking Prevention And Tobacco Control ACT, 2009. In: CONGRESS, U.S. (Ed.), Pub.L. 111–31, H.R. 1256.

Flecknell, P., 2002. Replacement, reduction and refinement. ALTEX 19, 73–78.

Fok, W.C., Bokov, A., Gelfond, J., Yu, Z., Zhang, Y., Doderer, M., Chen, Y., Javors, M., Wood, W.H., Zhang, Y., 2014. Combined treatment of rapamycin and dietary restriction has a larger effect on the transcriptome and metabolome of liver. Aging Cell 13, 311–319.

Furuse, M., Hata, M., Furuse, K., Yoshida, Y., Haratake, A., SUgitani, Y., Noda, T., Kubo, A., TSukita, S., 2002. Claudin-based tight junctions are crucial for the mammalian epidermal barrier: a lesson from claudin-1-deficient mice. J. Cell Biol. 156, 1099–1111.

Genco, R.J., 1996. Current view of risk factors for periodontal diseases. J. Periodontol. 67, 1041–1049.

Genco, R.J., Borgnakke, W.S., 2013. Risk factors for periodontal disease. Periodontology 2000 (62), 59–94.

Gentleman, R.C., Carey, V.J., Bates, D.M., Bolstad, B., Dettling, M., Dudoit, S., Ellis, B., Gautier, L., Ge, Y., Gentry, J., 2004. Bioconductor: open software development for computational biology and bioinformatics. Genome Biol. 5, R80.

Giannopoulou, C., Cappuyns, I., Mombelli, A., 2003a. Effect of smoking on gingival crevicular fluid cytokine profile during experimental gingivitis. J. Clin. Periodontol. 30, 996–1002.

Giannopoulou, C., Kamma, J.J., Mombelli, A., 2003b. Effect of inflammation, smoking and stress on gingival crevicular fluid cytokine level. J. Clin. Periodontol. 30, 145–153.

Goldkorn, T., Filosto, S., Chung, S., 2014. Lung injury and lung cancer caused by cigarette smoke-induced oxidative stress: molecular mechanisms and therapeutic opportunities involving the ceramide-generating machinery and epidermal growth factor receptor. Antioxid. Redox Signal 21, 2149–2174.

Gualerzi, A., Sciarabba, M., Tartaglia, G., Sforza, C., Donetti, E., 2012. Acute effects of cigarette smoke on three-dimensional cultures of normal human oral mucosa. Inhal. Toxicol. 24, 382–389.

Guentsch, A., Preshaw, P.M., Bremer-Streck, S., Klinger, G., Glockmann, E., Sigusch, B.W., 2008. Lipid peroxidation and antioxidant activity in saliva of periodontitis patients: effect of smoking and periodontal treatment. Clin. Oral Investig. 12, 345–352.

Hai, R., Chu, A., Li, H., Umamoto, S., Rider, P., Liu, F., 2006. Infection of human cytomegalovirus in cultured human gingival tissue. Virol. J. 3, 84.

Hasegawa, M., Nelson, H.H., Peters, E., Ringstrom, E., Posner, M., Kelsey, K.T., 2002. Patterns of gene promoter methylation in squamous cell cancer of the head and neck. Oncogene 21, 4231–4236.

Health Canada, 1999. Determination of tar, water, nicotine and carbon monoxide in mainstream tobacco smoke. Health Can. Test. Method T-11.

Henriksson, P., Hamberg, M., Diczfalusy, U., 1985. Formation of 15-HETE as a major hydroxyeicosatetraenoic acid in the atherosclerotic vessel wall. Biochimica Biophysica Acta (BBA)-Lipids Lipid Metabolism 834, 272–274.

Henry, J., Toulza, E., Hsu, C.Y., Pellerin, L., Balica, S., Mazereeuw-Hautier, J., paul, C., Serre, G., Jonca, N., Simon, M., 2012. Update on the epidermal differentiation complex. Front. Biosci. (Landmark Ed. 17, 1517–1532.

Hirohashi, S., Kanai, Y., 2003. Cell adhesion system and human cancer morphogenesis. Cancer Sci. 94, 575–581.

Huang, H.Y., Chen, S.Z., Zhang, W.T., Wang, S.S., Liu, Y., Li, X., Sun, X., Li, Y.M., Wen, B., Lei, Q.Y., Tang, Q.Q., 2013. Induction of EMT-like response by BMP4 via upregulation of lysyl oxidase is required for adipocyte lineage commitment. Stem Cell Res. 10, 278–287.

Huber, W., Von Heydebreck, A., Sültmann, H., Poustka, A., Vingron, M., 2002. Variance stabilization applied to microarray data calibration and to the quantification of differential expression. Bioinformatics 18, S96–S104.

Hultin-rosenberg, L., Forshed, J., Branca, R.M., Lehtio, J., Johansson, H.J., 2013.

Defining, comparing, and improving iTRAQ quantification in mass spectrometry proteomics data. Mol. Cell Proteomics 12, 2021–2031.
Inoue, M., 2016. Glutathionists in the battlefield of gamma-glutamyl cycle. Archives Biochem. biophysics 595, 61–63.
International Organization for Standardization, 1999. Tobacco and Tobacco Products – Atmosphere for Conditioning and Testing. Switzerland. http://www.iso.org/iso/home/store/catalogue_tc/catalogue_detail.htm?csnumber=28324.
Iskandar, A.R., Martin, F., Talikka, M., Schlage, W.K., Kostadinova, R., Mathis, C., Hoeng, J., Peitsch, M.C., 2013. Systems approaches evaluating the perturbation of xenobiotic metabolism in response to cigarette smoke exposure in nasal and bronchial tissues. Biomed. Res. Int. 2013, 512086.
Iskandar, A.R., Mathis, C., Martin, F., Leroy, P., Sewer, A., Majeed, S., Kuehn, D., Trivedi, K., Grandolfo, D., Cabanski, M., Guedj, E., Merg, C., Frentzel, S., Ivanov, N.V., Peitsch, M.C., Hoeng, J., 2016. 3-D nasal cultures: systems toxicological assessment of a candidate modified-risk tobacco product. ALTEX. Epub ahead of print.
Jacob, N., Golmard, J.L., Berlin, I., 2015. Relationships between nicotine and cotinine concentrations in maternal milk and saliva. Acta Paediatr. 104, e360, 6.
James, J.A., Sayers, N.M., Drucker, D.B., Hull, P.S., 1999. Effects of tobacco products on the attachment and growth of periodontal ligament fibroblasts. J. Periodontol. 70, 518–525.
Kanehisa, M., Goto, S., Sato, Y., Kawashima, M., Furumichi, M., Tanabe, M., 2014. Data, information, knowledge and principle: back to metabolism in KEGG. Nucleic acids Res. 42, D199–D205.
Kho, H.S., 2014. Understanding of xerostomia and strategies for the development of artificial saliva. Chin. J. Dent. Res. 17, 75–83.
Kim, S.G., Chae, C.H., Cho, B.O., Kim, H.N., Kim, H.J., Kim, I.S., Choi, J.Y., 2006. Apoptosis of oral epithelial cells in oral lichen planus caused by upregulation of BMP-4. J. Oral Pathol. Med. 35, 37–45.
Kimball, J.R., Nittayananta, W., Klausner, M., Chung, W.O., Dale, B.A., 2006. Antimicrobial barrier of an in vitro oral epithelial model. Arch. Oral Biol. 51, 775–783.
Kirkham, P.A., Barnes, P.J., 2013. Oxidative stress in COPD. Chest 144, 266–273.
Kogel, U., Schlage, W.K., Martin, F., Xiang, Y., Ansari, S., Leroy, P., Vanscheeuwijck, P., Gebel, S., Buettner, A., Wyss, C., Esposito, M., Hoeng, J., Peitsch, M.C., 2014. A 28-day rat inhalation study with an integrated molecular toxicology endpoint demonstrates reduced exposure effects for a prototypic modified risk tobacco product compared with conventional cigarettes. Food Chem. Toxicol. 68, 204–217.
Korashy, H.M., El-Kadi, A.O., 2012. Transcriptional and posttranslational mechanisms modulating the expression of the cytochrome P450 1A1 gene by lead in HepG2 cells: a role of heme oxygenase. Toxicology 291, 113–121.
Kose, O., Lalli, A., Kutulola, A.O., Odell, E.W., Waseem, A., 2007. Changes in the expression of stem cell markers in oral lichen planus and hyperkeratotic lesions. J. Oral Sci. 49, 133–139.
Koster, M.I., Roop, D.R., 2007. Mechanisms regulating epithelial stratification. Annu. Rev. Cell Dev. Biol. 23, 93–113.
Kundumani-Sridharan, V., Dyukova, E., Hansen, D.E., Rao, G.N., 2013. 12/15-Lipoxygenase mediates high-fat diet-induced endothelial tight junction disruption and monocyte transmigration a new role for 15 (S)-Hydroxyeicosatetraenoic acid in endothelial cell dysfunction. J. Biol. Chem. 288, 15830–15842.
Liberzon, A., Birger, C., Thorvaldsdóttir, H., Ghandi, M., Mesirov, J.P., Tamayo, P., 2015. The molecular signatures database hallmark gene set collection. Cell Syst. 1, 417–425.
Luo, L., Xie, P., Gong, P., Tang, X.H., Ding, Y., Deng, L.X., 2011. Expression of HMGB1 and HMGN2 in gingival tissues, GCF and PICF of periodontitis patients and peri-implantitis. Arch. Oral Biol. 56, 1106–1111.
Mahanonda, R., Sa-Ard-Iam, N., Eksomtramate, M., Rerkyen, P., Phairat, B., Schaecher, K.E., Fukuda, M.M., Pichyangkul, S., 2009. Cigarette smoke extract modulates human beta-defensin-2 and interleukin-8 expression in human gingival epithelial cells. J. Periodontal Res. 44, 557–564.
3RD Mahoney, M.G., Hu, Y., Brennan, D., Bazzi, H., Christiano, A.M., Wahl, J.K., 2006. Delineation of diversified desmoglein distribution in stratified squamous epithelia: implications in diseases. Exp. Dermatol 15, 101–109.
Majeed, S., Frentzel, S., Wagner, S., Kuehn, D., Leroy, P., Guy, P.A., Knorr, A., Hoeng, J., Peitsch, M.C., 2014. Characterization of the Vitrocell(R) 24/48 in vitro aerosol exposure system using mainstream cigarette smoke. Chem. Cent. J. 8, 62.
Malpass, G.E., Arimilli, S., Prasad, G.L., Howlett, A.C., 2013. Complete artificial saliva alters expression of proinflammatory cytokines in human dermal fibroblasts. Toxicol. Sci. 134, 18–25.
Martin, F., Sewer, A., Talikka, M., Xiang, Y., Hoeng, J., Peitsch, M.C., 2014. Quantification of biological network perturbations for mechanistic insight and diagnostics using two-layer causal models. BMC Bioinforma. 15, 238.
Mejia, A.B., Ling, P.M., Glantz, S.A., 2010. Quantifying the effects of promoting smokeless tobacco as a harm reduction strategy in the USA. Tob. Control 19, 297–305.
Mirowsk, G.W., Lozada-nur, F., Dekker, N.P., Macphail, L.A., Regezi, J.A., 1996. Altered expression of epithelial integrins and extracellular matrix receptors in oral erythema multiforme. J. Cutan. Pathol. 23, 473–478.
Mitchell, D., Paniker, L., Godar, D., 2012. Nucleotide excision repair is reduced in oral epithelial tissues compared with skin. Photochem Photobiol. 88, 1027–1032.
Moharamzadeh, K., Franklin, K.L., Brook, I.M., Van, N.,R., 2009. Biologic assessment of antiseptic mouthwashes using a three-dimensional human oral mucosal model. J. Periodontol. 80, 769–775.
Monnouchi, S., Maeda, H., Yuda, A., Serita, S., Wada, N., Tomokiyo, A., Akamine, A., 2016. Benzo[a]pyrene/aryl hydrocarbon receptor signaling inhibits osteoblastic differentiation and collagen synthesis of human periodontal ligament cells. J. Periodontal Res. 51, 779–788.
Morita, K., Miyachi, Y., Furuse, M., 2011. Tight junctions in epidermis: from barrier to keratinization. Eur. J. Dermatol 21, 12–17.
Mosharov, E., Cranford, M.R., Banerjee, R., 2000. The quantitatively important relationship between homocysteine metabolism and glutathione synthesis by the transsulfuration pathway and its regulation by redox changes. Biochemistry 39, 13005–13011.
Muller, W., Schroeder, H.E., 1980. Differentiation of the epithelium of the human hard palate. Cell Tissue Res. 209, 295–313.
Nam, D., Kim, S.-Y., 2008. Gene-set approach for expression pattern analysis. Briefings Bioinforma. 9, 189–197.
Nogueira, A.V., De souza, J.A., De molon, R.S., Pereira Eda, S., De Aquino, S.G., Giannobile, W.V., Cirelli, J.A., 2014. HMGB1 localization during experimental periodontitis. Mediat. Inflamm. 2014, 816320.
Ojima, M., Hanioka, T., 2010. Destructive effects of smoking on molecular and genetic factors of periodontal disease. Tob. Induc. Dis. 8, 4.
Omiecinski, C.J., Vanden Heuvel, J.P., Perdew, G.H., Peters, J.M., 2011. Xenobiotic metabolism, disposition, and regulation by receptors: from biochemical phenomenon to predictors of major toxicities. Toxicol. Sci. 120 (Suppl. 1), S49–S75.
Orellana-bustos, A.I., Espinoza-santander, I.L., Franco-Martinez, M.E., Lobos-James-Freyre, N., Ortega-Pinto, A.V., 2004. Evaluation of keratinization and AgNORs count in exfoliative cytology of normal oral mucosa from smokers and non-smokers. Med. Oral 9, 197–203.
Ozcaka, O., Bicakci, N., Pussinen, P., Sorsa, T., Kose, T., Buduneli, N., 2011. Smoking and matrix metalloproteinases, neutrophil elastase and myeloperoxidase in chronic periodontitis. Oral Dis. 17, 68–76.
Phillips, B., Esposito, M., Verbeeck, J., Boue, S., Iskandar, A., Vuillaume, G., Leroy, P., Krishnan, S., Kogel, U., Utan, A., Schlage, W.K., Bera, M., Veljkovic, E., Hoeng, J., Peitsch, M.C., Vanscheeuwijck, P., 2015. Toxicity of aerosols of nicotine and pyruvic acid (separate and combined) in Sprague-Dawley rats in a 28-day OECD 412 inhalation study and assessment of systems toxicology. Inhal. Toxicol. 27, 405–431.
Plackova, A., Skach, M., 1975. Fine structural study of keratinization of the filiform papillae in the tongue in humans. Z Mikrosk Anat. Forsch 89, 305–318.
Popat, R.V., Bhavsar, N.V., Popat, P.R., 2014. Gingival crevicular fluid levels of Matrix Metalloproteinase-1 (MMP-1) and Tissue Inhibitor of Metalloproteinase-1 (TIMP-1) in periodontal health and disease. Singap. Dent. J. 35, 59–64.
Powell, W.S., Rokach, J., 2015. Biosynthesis, biological effects, and receptors of hydroxyeicosatetraenoic acids (HETEs) and oxoeicosatetraenoic acids (oxo-ETEs) derived from arachidonic acid. Biochim. Biophys. Acta 1851, 340–355.
Preetha, A., Banerjee, R., 2005. Comparison of artificial saliva substitutes. Trends Biomater. Artif. Organs 18 (2).
Rodu, B., 2011. The scientific foundation for tobacco harm reduction, 2006-2011. Harm Reduct. J. 8, 19.
Romanelli, R., Mancini, S., Laschinger, C., Overall, C.M., Sodek, J., Mcculloch, C.A., 1999. Activation of neutrophil collagenase in periodontitis. Infect. Immun. 67, 2319–2326.
Rovida, C., Asakura, S., Daneshian, M., Hofman-Huether, H., Leist, M., Meunier, L., Reif, D., Rossi, A., Schmutz, M., Valentin, J.P., Zurlo, J., Hartung, T., 2015. Toxicity testing in the 21st century beyond environmental chemicals. ALTEX 32, 171–181.
Russell, W.M.S., Burch, R.L., Hume, C.W., 1959. The principles of humane experimental technique.
Saito, K., Maekawa, K., Kinchen, J.M., Tanaka, R., Kumagai, Y., Saito, Y., 2016. Gender- and age-associated differences in serum metabolite profiles among Japanese Populations. Biol. Pharm. Bull. 39, 1179–1186.
Sapna, G., Gokul, S., Bagri-Manjrekar, K., 2014. Matrix metalloproteinases and periodontal diseases. Oral Dis. 20, 538–550.
Schaller, J.-P., Keller, D., Poget, L., Pratte, P., Kaelin, E., Mchugh, D., Cudazzo, G., Smart, D., Tricker, A.R., Gautier, L., 2016. Evaluation of the Tobacco Heating System 2.2. Part 2: chemical composition, genotoxicity, cytotoxicity, and physical properties of the aerosol. Regul. Toxicol. Pharmacol. 81 (Suppl 2), S27–S47.
Scheller, J., Chalaris, A., Schmidt-Arras, D., Rose-John, S., 2011. The pro- and anti-inflammatory properties of the cytokine interleukin-6. Biochim. Biophys. Acta 1813, 878–888.
Schlage, W.K., Iskandar, A.R., Kostadinova, R., Xiang, Y., Sewer, A., Majeed, S., Kuehn, D., Frentzel, S., Talikka, M., Geertz, M., Mathis, C., Ivanov, N., Hoeng, J., Peitsch, M.C., 2014. In vitro systems toxicology approach to investigate the effects of repeated cigarette smoke exposure on human buccal and gingival organotypic epithelial tissue cultures. Toxicol. Mech. Methods 24, 470–487.
Semlali, A., Chakir, J., Goulet, J.P., Chmielewski, W., Rouabhia, M., 2011. Whole cigarette smoke promotes human gingival epithelial cell apoptosis and inhibits cell repair processes. J. Periodontal Res. 46, 533–541.
Serhan, C.N., Jain, A., Marleau, S., Clish, C., Kantarci, A., Behbehani, B., Colgan, S.P., Stahl, G.L., Merched, A., Petasis, N.A., Chan, L., Van dyke, T.E., 2003. Reduced inflammation and tissue damage in transgenic rabbits overexpressing 15-lipoxygenase and endogenous anti-inflammatory lipid mediators. J. Immunol. 171, 6856–6865.
Sheldon, L.S., Cohen Hubal, E.A., 2009. Exposure as part of a systems approach for assessing risk. Environ. Health Perspect. 117, 119–1194.
Shetty, S., Gokul, S., 2012. Keratinization and its disorders. Oman Med. J. 27,

348–357.
Shirani, S., Kargahi, N., Razavi, S.M., Homayoni, S., 2014. Epithelial dysplasia in oral cavity. Iran. J. Med. Sci. 39, 406–417.
Singh, B.B., Schuster, G.S., Merchant, V.A., Michelich, V.J., 1979. Ultrastructural and autoradiographic observations of hamster cheek pouch epithelium grown in vitro. Vitro 15, 865–872.
Smith, M.R., Clark, B., Ludicke, F., Schaller, J.P., Vanscheeuwijck, P., Hoeng, J., Peitsch, M.C., 2016. Evaluation of the tobacco heating system 2.2. Part 1: description of the system and the scientific assessment program. Regul. Toxicol. Pharmacol. 81 (Suppl 2), S17–S26.
Stratton, K., Shetty, P., Wallace, R., Bondurant, S., 2001. Clearing the Smoke: Assessing the Science Base for Tobacco Harm Reduction. Washington (DC).
Su, L., Morgan, P.R., Thomas, J.A., Lane, E.B., 1993. Expression of keratin 14 and 19 mRNA and protein in normal oral epithelia, hairy leukoplakia, tongue biting and white sponge nevus. J. Oral Pathol. Med. 22, 183–189.
Sugiyama, A., Uehara, A., Iki, K., Matsushita, K., Nakamura, R., Ogawa, T., Sugawara, S., Takada, H., 2002. Activation of human gingival epithelial cells by cell-surface components of black-pigmented bacteria: augmentation of production of interleukin-8, granulocyte colony-stimulating factor and granulocyte-macrophage colony-stimulating factor and expression of intercellular adhesion molecule 1. J. Med. Microbiol. 51, 27–33.
Sweanor, D., Alcabes, P., Drucker, E., 2007. Tobacco harm reduction: how rational public policy could transform a pandemic. Int. J. Drug Policy 18, 70–74.
Tamaki, N., Cristina Orihuela-campos, R., Inagaki, Y., Fukui, M., Nagata, T., Ito, H.O., 2014. Resveratrol improves oxidative stress and prevents the progression of periodontitis via the activation of the Sirt1/AMPK and the Nrf2/antioxidant defense pathways in a rat periodontitis model. Free Radic. Biol. Med. 75, 222–229.
Toulza, E., Mattiuzzo, N.R., Galliano, M.F., Jonca, N., Dossat, C., Jacob, D., De daruvar, A., Wincker, P., Serre, G., Guerrin, M., 2007. Large-scale identification of human genes implicated in epidermal barrier function. Genome Biol. 8, R107.
Tsai, C.C., Chen, H.S., Chen, S.L., Ho, Y.P., Ho, K.Y., Wu, Y.M., Hung, C.C., 2005. Lipid peroxidation: a possible role in the induction and progression of chronic periodontitis. J. Periodontal Res. 40, 378–384.
Tsang, S.M., Brown, L., Lin, K., Liu, L., Piper, K., O'toole, E.A., Grose, R., Hart, I.R., Garrod, D.R., Fortune, F., Wan, H., 2012. Non-junctional human desmoglein 3 acts as an upstream regulator of Src in E-cadherin adhesion, a pathway possibly involved in the pathogenesis of pemphigus vulgaris. J. Pathol. 227, 81–93.
Tucci, P., Porta, G., Agostini, M., Dinsdale, D., Iavicoli, I., Cain, K., Finazzi-agró, A., Melino, G., Willis, A., 2013. Metabolic effects of TiO2 nanoparticles, a common component of sunscreens and cosmetics, on human keratinocytes. Cell death Dis. 4, e549.
Villar, C.C., De lima, A.F., 2003. Smoking influences on the thickness of marginal gingival epithelium. Pesqui. Odontol. Bras. 17, 41–45.
Villar, C.C., Lima, A.F.M.D., 2003. Smoking influences on the thickness of marginal gingival epithelium. Pesqui. Odontológica Bras. 17, 41–45.
Vondracek, M., Xi, Z., Larsson, P., Baker, V., Mace, K., Pfeifer, A., Tjalve, H., Donato, M.T., Gomez-lechon, M.J., Grafstrom, R.C., 2001. Cytochrome P450 expression and related metabolism in human buccal mucosa. Carcinogenesis 22, 481–488.
Yang, J., Deol, G., Myangar, N., 2011. Retention of o-cymen-5-ol and zinc on reconstructed human gingival tissue from a toothpaste formulation. Int. Dent. J. 61 (Suppl. 3), 41–45.
Ye, P., Chapple, C.C., Kumar, R.K., Hunter, N., 2000. Expression patterns of E-cadherin, involucrin, and connexin gap junction proteins in the lining epithelia of inflamed gingiva. J. Pathol. 192, 58–66.
Yoshizawa, M., Koyama, T., Kojima, T., Kato, H., Ono, Y., Saito, C., 2012. Keratinocytes of tissue-engineered human oral mucosa promote re-epithelialization after intraoral grafting in athymic mice. J. Oral Maxillofac. Surg. 70, 1199–1214.
YU, Y., Tang, D., Kang, R., 2015. Oxidative stress-mediated HMGB1 biology. Front. Physiol. 6, 93.
Yuki, D., Kikuchi, A., Miura, N., Kakehi, A., Onozawa, M., 2013. Good relationship between saliva cotinine kinetics and plasma cotinine kinetics after smoking one cigarette. Regul. Toxicol. Pharmacol. 67, 240–245.
Zanetti, F., Sewer, A., Mathis, C., Iskandar, A.R., Kostadinova, R., Schlage, W.K., Leroy, P., Majeed, S., Guedj, E., Trivedi, K., Martin, F., Elamin, A., Merg, C., Ivanov, N.V., Frentzel, S., Peitsch, M.C., Hoeng, J., 2016. Systems toxicology assessment of the biological impact of a candidate Modified Risk Tobacco Product on human organotypic oral epithelial cultures. Chem. Res. Toxicol. 29, 1252–1269.
Zeller, M., Hatsukami, D., Strategic dialogue on tobacco harm reduction, G, 2009. The strategic dialogue on tobacco harm reduction: a vision and blueprint for action in the us. Tob. Control 18, 324–332.
Zhou, K., Muroyama, A., Underwood, J., Leylek, R., Ray, S., Soderling, S.H., Lechler, T., 2013. Actin-related protein2/3 complex regulates tight junctions and terminal differentiation to promote epidermal barrier formation. Proc. Natl. Acad. Sci. U. S. A. 110, E3820–E3829.